

1 **Regionalisation of Rainfall Depth-Duration-Frequency curves in** 2 **with different data types in Germany**

3 B. Shehu¹, W. Willems², H. Stockel², L. Thiele¹, U. Haberlandt¹

4 ¹ Institute of Hydrology and Water Resources Management, Leibniz University Hannover Germany

5 ² IAWG, Engineering Hydrology, Applied Water Resources and Geoinformatics, Ottobrunn Germany

6 *Correspondence to: Bora Shehu (shehu@iww.uni-hannover.de)*

7 **Abstract.**

8 Rainfall depth-duration-frequency (DDF) curves are required for the design of several water systems and protection
9 works. ~~These curves are typically generated from the station data by fitting a theoretical distribution to the annual extremes~~
10 ~~(AMS). The aim of this study is to investigate the use of different data types and methods for estimating reliable DDF~~
11 ~~curves covering whole Germany. The following three questions are investigated for the evaluation and regionalisation of~~
12 ~~the DDF curves in Germany: i) which is the best local estimation method, ii) which regionalisation method shows best~~
13 ~~performance, and iii) which data sets should be used and how they should be integrated. For reliable estimation of such~~
14 ~~curves, long and dense observation networks are necessary, which in practice are seldom the case. Usually observations~~
15 ~~with different accuracy, temporal resolution and density are present. In this study, we investigate the integration of~~
16 ~~different observation data sets under different methods for the local and regional estimation of DDF curves in Germany.~~

17 For this purpose, two competitive DDF-procedures for local estimation (Koutsoyiannis et al. 1998, Fischer and
18 Schumann, 2018) and two for regional estimation (kriging theory vs index-based) are implemented and compared.
19 Available station data from the German Weather Service (DWD) for Germany are employed, which includes; 5000 daily
20 stations with more than 40 years available, 1261 high resolution (1min) recordings with observations period between 10
21 and 20 years, and finally 133 high resolution (1min) recordings with 60-70 years of observations. The performance of the
22 selected approaches is evaluated by cross-validation, where the local DDFs from the long sub-hourly time series are
23 considered the true reference. The results reveal that the best approach for the estimation of the DDF curves in Germany
24 is by first deriving the local extreme value statistics based on Koutsoyiannis et al. 1998 framework, and later using the
25 kriging regionalisation of long sub-hourly time series with the short sub-hourly time series acting as an external drift. The
26 integration of the daily stations proved to be useful only for DDF values of very-low return period ($T < 10$ years), but not
27 doesn't introduce any improvement for higher return periods ($T \geq 10$ years).

28 **Keywords:**

29 Depth-Duration-Frequency, Regionalisation, Disaggregation, Kriging, Index-based

Formatted: Not Highlight

30 **1. Introduction**

31 Rainfall volumes at varying duration and frequencies are required for the design of water management systems and
32 facilities, like dams or dikes, spillways, flood retention basins, urban drainage systems, etc. These design precipitation
33 volumes are also known as IDF (Intensity-Duration-Frequency) or DDF (Depth-Duration-Frequency) curves, and are
34 derived from an extreme value analysis (EVA) on observed rainfall. For sampling extreme values, either annual maximum
35 series (AMS) or peak-over-threshold (POT) can be used, however for return periods greater than 10 years, there are hardly
36 any differences between the two. Often the AMS are preferred over the POT because the methodology is more direct and
37 easier, whereas the POT method needs a prior assumption on the threshold selection. Afterwards a theoretical probability
38 distribution (PDF) is fitted to the extreme series of a certain duration, in order to extract design rainfall volumes at specific
39 frequency (or return periods). Typically, a Generalized Extreme Value (GEV) distribution is fitted for the AMS series
40 and a Generalised Pareto for the POT series extracted for a fixed duration level. Rainfall extremes of different durations
41 are strongly related to each other, however, if the parameter fitting is done independently to each duration level these
42 relations may not be kept (Cannon, 2018). Therefore, generalised concepts as in (Koutsoyiannis et al., 1998), simple
43 scaling (Gupta and Waymire, 1990) or multi scaling Van de Vyver (2015) approaches are used to smooth the extreme
44 statistics over different duration levels. Finally, since the rainfall observations are mostly point measurements, a
45 regionalisation procedure of the PDF parameters to un-observed locations is performed. Methodologically, a distinction
46 can be made between two approaches: a) a direct regionalisation of quantiles, moments or parameters of distribution
47 functions and b) a regional estimation of distribution functions for homogeneous regions. Borga et al. (2005) suggests the
48 regionalisation of the parameters instead of the quantiles. For the direct regionalisation of parameters, regressions
49 (Madsen et al., 2009; Smithers and Schulze, 2001), splines (Johnson and Sharma, 2017) or kriging methods (Ceresetti et
50 al., 2012; Kebaili Bargaoui and Chebbi, 2009; Uboldi et al., 2014; Watkins et al., 2005) are applied. On the other hand,
51 the estimation of regional distributions functions based on the index method proposed by Hosking and Wallis (1997), is
52 one of the most used methods in the literature for the regionalisation of design precipitation (Burn, 2014; Durrans and
53 Kirby, 2004; Forestieri et al., 2018; De Salas and Fernández, 2007).

54 Rainfall volumes at varying duration and frequencies are required for the design of water management systems and
55 facilities, like dams or dikes, spillways, flood retention basins, urban drainage systems, etc. These design precipitation
56 volumes are also known as IDF (Intensity-Duration-Frequency) or DDF (Depth-Duration-Frequency) curves. The main
57 application of the DDF curves is the derivation of design discharge from design rainfall, when no sufficient discharge
58 observations are available assuming that both rainfall and discharge events have the same recurrence interval (herein
59 referred to as return period T_a). For sampling, the annual maximum series (AMS) or peak-over threshold (POT) can be
60 used, however for return periods greater than 10 years, there are hardly any differences in the results obtained from each
61 method. Often the AMS are preferred over the POT because the methodology is more direct and easier, whereas the POT
62 method needs a prior assumption on the threshold selection. The typical procedure includes fitting a theoretical probability
63 distribution (PDF) to the observed rainfall extremes at a certain duration level, and based on the obtained PDF, compute
64 the quantiles corresponding to different return periods. Most common distribution functions are Generalised Extreme
65 Value (GEV), Gumbel, Log-Pearson III and Lognormal distributions for AMS, with GEV and Gumbel being the most
66 popular, and Generalised Pareto for POT. L-moments are primarily used for parameter estimation in recent national
67 applications (Johnson and Sharma, 2017). Since the estimation of extreme design rainfall is done locally at each
68 measurement station (rain-gauge), a regionalisation method, often the index-flood method (herein referred the index
69 method) is employed to estimate design rainfall depth at ungauged location (Hosking and Wallis, 1997). In Germany, the
70 Coordinated Heavy Rainfall Regionalisation Evaluation KOSTRA DWD (Malitz and Ertel, 2015) from the German
71 Weather Service (DWD) has been providing these design precipitation volumes for different application purposes since

Formatted: Font color: Black
Formatted: Normal, No bullets or numbering

Formatted: Font color: Black

Formatted: Font color: Black

Formatted: Not Highlight

Formatted: Font color: Black

1980. A revision of the KOSTRA-DWD is required, in order to consider the recent state of the art and additional data. Therefore, it is the aim of this study to investigate the use of different methods for the estimation and regionalisation of the DDF curves and the best integration of different data types, in order to give the basis for the development of the new regional design rainfall catalogue for Germany. In this procedure, several research questions arise which are discussed below:

i) Local estimation

A prominent probability distribution that is frequently used in the statistical analysis of AMS of heavy rainfall is the Gumbel distribution. The Gumbel distribution is a special case of the three-parameter GEV distribution where the shape parameter is zero ($\gamma=0$) and the distribution follows an exponential tail behaviour. If the shape parameter is greater than zero, the distribution exhibits a so-called heavy-tail behaviour (also known as GEV type II), whilst if the shape parameter is less than zero no tail behaviour is present (also known as GEV type III) (Coles, 2001). The GEV type III is not employed in rainfall extreme value statistics, as it is bounded from above. The Gumbel and the GEV type II (herein referred to as simply GEV) are almost similar for low percentiles, nevertheless diverge greatly for high return periods. Therefore, for the design rainfall at high return periods, the expression of the shape parameter is of decisive importance. Regarding this issue, extensive investigations were carried out to determine the role of the shape parameter in heavy precipitation data, both in a theoretical manner and on the basis of empirical findings. For instance, Koutsoyiannis (2004a) investigated the heavy-tail behaviour of extreme daily rainfall values at 169 worldwide locations with very long observations (100-150 years) and concluded that when only short observations are present (less than 50 years) the heavy-tail characteristics can be overlooked and the Gumbel distribution is chosen falsely as a good fit. This may be also the reason why for a long time in the literature mainly the Gumbel distribution was preferred. Koutsoyiannis (2004b) proposed a GEV distribution with a shape parameter fixed within the range $\gamma=0.1-0.15$ for all examined geographical zones (mainly in Europe and North America). Specifically, he proposes the value of 0.15 if very high return periods are of interest, and the value of 0.1 if the focus is also on low return periods. Later, Papalexiou and Koutsoyiannis (2013) analysed more than 15,000 stations worldwide with observation length from 40 to 160 years, and again the results favoured the implementation of heavy-tail GEV distribution instead of the Gumbel. A recent study by Papalexiou (2018) on hourly rainfall measurements in the USA, suggested that also for sub-daily durations, the rainfall extremes exhibit a heavy-tail (sub-exponential), much heavier than the exponential or the Gamma tails. Mountain areas tend to exhibit heavier tails; however, terrain is not the dominant factor influencing the tail behaviour. Overall, the analysis suggests that the shape parameter cannot be evaluated adequately when the station's recordings are short and from a Gumbel distribution, therefore the GEV should be used instead.

To determine the design rainfall, distribution functions are usually first fitted separately for each of the selected duration levels. This way, quantile crossing may arise between different duration levels (Cannon, 2018). Quantile crossing here refers to when the extreme rainfall volumes for a fixed return period (say $T_a=100$ years) are not increasing with longer duration levels. Theoretically, the rainfall volume is dependent on the duration and thus another step in the extreme value analysis is needed, to ensure that the extremes are consistently increasing with the duration levels. An empirical relationship was first developed by Bernard (1932), where the intensities at different duration levels are generalised by a power law depending on three location constants. (Koutsoyiannis et al., 1998) proposed a similar mathematical framework, where the AMS intensities are generalised based on two parameters ($\theta > 0$ and $0 < \eta < 1$) and a probability distribution function (PDF) is fitted based on these generalised intensities to estimate the quantiles for specific return periods. The generalised concept suggested by Koutsoyiannis has widely been implemented in the literature (Asikoglu and Benzedden, 2014; Muller et al., 2008; Ulrich et al., 2021; Van de Vyver, 2015). Ulrich et al. (2021) implemented such

113 a framework in Germany for both monthly and annual IDF's curve, with a constant shape parameter of 0.11 for the annual
114 estimation. Another alternative application is based on the wide sense scaling theory, where the PDF parameters or
115 moments of each duration are dependable on a power law (Gupta and Waymire, 1990). Van de Vyver (2015) implemented
116 a multi-scaling approach, where both the location and the scale parameters of duration specific GEV were related on a
117 power law with the duration, while the shape parameter was kept constant. Similar approaches were also proposed and
118 studied by Haktanir et al. (2010), Holešovský et al. (2016), Soulis et al. (2016), and are typically referred to as smoothing
119 of extreme statistics over the duration levels.

120 Other solutions build also on the power law relationship between extremes and durations are for instance Bayesian
121 distribution models (Boukhelifa et al., 2018; Lima et al., 2016; Roksvåg et al., 2021; Van de Vyver, 2018), marginal
122 probabilities (Veneziano et al., 2007), and artificial intelligence (Cannon, 2018). An alternative approach for achieving a
123 DDF based on data from example of such implementation in Germany was proposed by Fischer and Schumann (2018),
124 where location and scale parameters are obtained by a regression model (based on a nonlinear least squares method), and
125 the shape parameter is estimated indirectly by quantifying first the normalised scale/shape ratio with a robust linear
126 regression. Here we consider the two approaches of Koutsoyiannis et al. (1998) and Fischer and Schumann (2018), as
127 they have successfully been tested in Germany. Here, the question remains whether a homogenisation of intensities or a
128 smoothing of GEV parameters across different duration levels is more appropriate for the estimation of the DDF curves
129 in Germany.

130 ii) ——— Regionalisation methods

131 Regionalisation of the design DDF curves provides estimation for unobserved locations, but also contributes to a more
132 robust estimation, e.g. by using larger samples (Requena et al., 2019). Methodologically, a distinction can be made
133 between two approaches: a) a direct regionalisation of quantiles, moments or parameters of distribution functions and b)
134 a regional estimation of distribution functions for homogeneous regions. A direct regionalisation of quantiles may lead
135 as well to quantile crossing across durations, and therefore mostly regionalisation of parameters is performed. Furthermore
136 Borga et al. (2005) suggests the regionalisation of the parameters instead of the quantiles. For the direct regionalisation
137 of parameters, regressions (Madsen et al., 2009; Smithers and Schulze, 2001), splines (Johnson and Sharma, 2017) or
138 geostatistical methods (Ceresetti et al., 2012; Kebaili Bargaoui and Chebbi, 2009; Uboldi et al., 2014; Watkins et al.,
139 2005) are applied. On the other hand, the estimation of regional distributions functions based on the index method
140 proposed by Hosking and Wallis (1997), is one of the most used methods in the literature for the regionalisation of design
141 precipitation (Burn, 2014; Durrans and Kirby, 2004; Forestieri et al., 2018; De Salas and Fernández, 2007). Many
142 countries have actually employed the index based regionalisation for estimation of regional IDF/DDF curves, for instance
143 Canada (Burn, 2014), Denmark (Madsen et al., 2009) and USA (Perica et al., 2019). However, prior to the application
144 of the index method, it is important to define adequately homogeneous regions where the rainfall statistics are similar,
145 which can be a challenging task (De Salas and Fernández, 2007). Hosking and Wallis, (1997) recommend that site
146 characteristics should be used for the identification of homogeneous regions instead of site statistics. Therefore, the second
147 objective of this paper is to investigate whether a direct kriging interpolation of the GEV parameters or the application of
148 the index method on homogeneous regions is more suitable for the estimation of regional DDF curves in Germany.

149 iii) ——— Combination of available datasets with different temporal resolution and observation length

150 As stated in Koutsoyiannis (2004a,b) short time series can choose Gumbel parameters falsely and hide the true heavy tail
151 behaviour of rainfall extremes. Thus, care should be taken when combining different statistics from different observation
152 lengths. Madsen et al., (2017) investigated the IDF curves with long stations (more than 40 years) and short stations (less
153 than 30 years) based on Generalised Pareto distribution with fix shape parameter, and concluded that the statistics are

154 changing from one case to the other, with short series giving large estimates of the extreme intensities. This of course can
155 be attributed to the non-stationarity of the IDF curves. Holešovský et al. (2016) separated the historical data into groups
156 when estimating IDF curves for Czech Republic (long series with 35-40 and short series with 11-15 years of observations),
157 and concluded that the uncertainty at estimating parameters for the short time series is quite high, especially for high
158 return periods. In the index-based regionalisation, regional L-moments are averaged based on the observation length,
159 which may lead to more stable results (Burn, 2014; Requena et al., 2019), however the interpolated index may still suffer
160 from high uncertainties from pooling together short and long time series. This may also be the case when interpolating
161 local GEV parameters with the kriging theory. Therefore, it is important to investigate which is the best combination of
162 time series with different observation length: even though the short time series may be not adequate for high return period
163 quantiles, they are much denser than the longer time series. Hence their information may be helpful in trading space for
164 time.

165 In Addition to the high resolution (1-5min) network, the daily one is much denser and as well with very long observation
166 lengths. Nevertheless, the temporal resolution is too coarse for the estimation of sub-hourly to sub-daily extremes. In such
167 cases, GEV parameters for the sub-daily duration can be scaled from the GEV parameters of the daily extremes following
168 the scale invariance principle of precipitation extremes. Bara et al. (2009) employed the scale invariance principle to
169 derive DDF curves for sub-daily duration levels (5min – 3h) from daily observations in Slovakia, while Borga et al. (2005)
170 applied two different scaling factors one for duration levels less than 1 hour and one for longer than 1 hour in northern-
171 eastern Italy. A later study from Paixao et al. (2011) performed in Ontario Canada concluded that the scaling factors
172 should not be used for reliable downscaling of daily extremes to durations less or equal to one hour. This is because the
173 extremes at such short durations are governed by other rainfall mechanisms than the daily extremes, and hence a low
174 dependency exists between the two extreme groups. Alternative to the scale invariance principle, disaggregation schemes
175 can be applied to the daily data in order to obtain high resolution data. Various model approaches for disaggregation are
176 described in the literature, and they mostly consist of a so-called cascade model (Müller and Haberlandt, 2018). Weather
177 radar data can be used to estimate the probabilities in the individual levels and to derive the extensive parameter sets
178 suggested by Lisniak et al. (2013) for the disaggregation scheme. Therefore, the third objective of the paper is to
179 investigate the value and the best combination of data from the long, short and disaggregated daily series for the
180 regionalisation of the DDF curves in Germany.

181 Since the analysis is performed on extreme values, first very long observations are required to ensure a proper fitting of
182 the GEV parameters, particularly of the shape parameter which is of decisive importance for extremes of high return
183 period (larger than 20 years return period). For instance, Koutsoyiannis (2004a,b) showed clearly that short time series
184 (less than 50 years) can choose falsely a shape parameter of zero (Gumbel distribution) and hide the true heavy-tail
185 behaviour of rainfall extremes (also supported by Papalexiou and Koutsoyiannis (2013) and Papalexiou (2018)). Second,
186 a dense observation network should be available to ensure an adequate estimation of extreme value statistics also at un-
187 observed locations. A less denser network would cause for instance that the kriging interpolated values to be less accurate
188 and the spatial features to be more smoothen in space (Berndt et al., 2014). On the other side, index-based regionalisation
189 can provide more robust estimation at un-observed locations if larger samples (obtained from denser networks) are used
190 (Requena et al., 2019). Third, a high-resolution observation network (with 1- or 5- time steps) is as well necessary to
191 estimate extremes of short durations (at scales of minutes or hours) for catchments that respond quickly to rainfall events
192 (i.e. urban or mountainous areas prone to flash floods). At the moment, no perfect observation network that fulfils these
193 three criteria is available, however different networks or datatypes fulfilling two criteria co-exist. For example, daily
194 observation networks are typically very dense (every 10km) and can have up to 100-150 years of observations, but don't
195 capture the extremes at sub-hourly durations. Digital tipping bucket or weighting sensors can measure the rainfall at 1min

Field Code Changed

196 [time steps and can be dense \(every 20-25km\), however they are available mostly after 2000 and hence too short for EVA.](#)
197 [Long observations at 1min time steps from analogous Hellmann or tipping buckets may be available from 1900-1950](#)
198 [only at some countries \(i.e. Germany, Belgium\) but are not as dense as digital or daily measurements \(>50km\).](#)
199 [Alternatively, weather radar or satellite data can provide rainfall fields at 1- or 4-km² and 5min time steps, but offer short](#)
200 [observations \(less than 20 years\) and suffer from high inaccuracies \(Marra et al., 2019\).](#)
201 [To optimize the DDF estimation, different data types have been combined for instance; Madsen et al., \(2017\) regionalised](#)
202 [extremes in Denmark from 1min observation with daily interpolated values as a co-variate, Bara et al. \(2009\) employed](#)
203 [the simple scale principle to derive DDF curves for sub-daily duration levels \(5min – 3h\) from daily observations in](#)
204 [Slovakia, Goudenhoofdt et al., \(2017\) used station observations \(10min and varying lengths\) to correct radar data and](#)
205 [estimate the hourly and daily extremes, Burn \(2014\) pooled together long and short observations at 5min time steps to](#)
206 [form the DDF curves in Canada. However, care should be taken when combining information from data types that differ](#)
207 [in observation length, temporal and spatial scales. Holešovský et al. \(2016\) separated the historical data into groups when](#)
208 [estimating DDF curves for Czech Republic \(long series with 35-40 and short series with 11-15 years of observations\),](#)
209 [and concluded that the uncertainty at estimating parameters for the short time series is quite high, especially for high](#)
210 [return periods. In the index-based regionalisation, regional L-moments are averaged based on the observation length,](#)
211 [which may lead to more stable results \(Burn, 2014; Requena et al., 2019\), however the interpolated index may still suffer](#)
212 [from high uncertainties from pooling together short and long time series. This may also be the case when interpolating](#)
213 [local GEV parameters with the kriging theory. The regionalisation of the shape parameter may be not representative if](#)
214 [short and long observations are pooled together with same importance, thus keeping a fix shape parameter may help to](#)
215 [mitigate this problem. Nevertheless, further investigation should be done to ensure if long observations, as more reliable,](#)
216 [should have more importance than the short ones when regionalising extreme value statistics. Regarding the temporal](#)
217 [scale difference, a study from Paixao et al. \(2011\) performed in Ontario Canada concluded that the scaling factors should](#)
218 [not be used for downscaling daily extremes to durations less or equal to one hour. This is because the extremes at such](#)
219 [short durations are governed by other rainfall mechanisms than the daily extremes, and hence a low dependency exists](#)
220 [between the two extreme groups. Alternative to the scaling principle, disaggregation schemes can be applied to the daily](#)
221 [data in order to obtain adequate extremes \(with return period up to 5 years\) for sub-hourly durations \(Müller and](#)
222 [Haberlandt, 2018\). On the other hand, because of the spatial scale inconsistency between weather radar and gauge](#)
223 [observations, the weather radar may not be appropriate to estimate directly extremes of short durations \(Marra et al.,](#)
224 [2019\), however they can still be useful to extract sub-daily extremes if used to disaggregate daily observations as done](#)
225 [by Bárdossy and Pegram \(2017\). More complex disaggregation procedures that take advantage of the radar information](#)
226 [by implementing an extensive parameter-set as suggested by Lisniak et al. \(2013\), may also be used to disaggregate daily](#)
227 [observation and estimate the extreme values at sub-hourly durations. Nevertheless, to authors knowledge, there is no](#)
228 [study in the literature that investigates if disaggregated daily time series can be useful in regionalising extreme values](#)
229 [statistics when high resolution data are present, and when so, if they should have the same weights as high-resolution](#)
230 [data.](#)
231 [Lastly, due to lack of data, in most of the literature, the combination of any two or alternative data types for EVA is](#)
232 [validated on observations that are not dense or long enough \(longer than 40-50 years\). Therefore, it would be interesting](#)
233 [to test different methods for estimation and regionalisation of DDF curves extracted from different datatypes, on a long](#)
234 [and dense network. The German Weather Service \(DWD\) has a relatively dense observations network \(every 50km\) of](#)
235 [1min rainfall data available from 1950 \(60-70years\), that enables a proper validation of EVA for return periods up to 100](#)
236 [years. Additionally, denser digital observations \(every 20km\) at 1min time steps \(mainly from 2000\), very dense \(every](#)
237 [10km\) daily observations \(10-120years\) and weather radar observations \(from 2000\) at 1km² and 5min time steps are as](#)

Formatted: Superscript

238 well available. As multiple data types co-exist in Germany, it is important to investigate the suitability of methods and
239 data types for the extraction and regionalisation of extreme statistics while validating only at the long and dense
240 observations. In Germany, studies either use the Koutsoyiannis approach or multi/simple scaling approach of GEV
241 parameters to generalise the extremes over different durations. To authors knowledge there is no comparison of the two
242 approaches in the literature. The Koutsoyiannis approach has been implemented in Germany by (Ulrich et al. (-2020),
243 but on a shorter available 1 min dataset (up to 14 years), while Fischer and Schumann (2018) have implemented the multi
244 scale approach only at a long station (~85 years). Here we investigate which of these methods gives more accurate and
245 precise estimation of DDF based on the long and 1min rainfall data. The same is true also for the regionalisation
246 approaches: to authors knowledge there is no comparison between kriging and index-based regionalisation. Naturally, it
247 is interesting to see which of the methods is more appropriate when validated on a long and high-resolution network, and
248 where lie the advantages and disadvantages of each method when different data types are integrated, and what
249 combination brings the best outcome. For this purpose, we investigate here three competitive regionalisation methods
250 (ordinary kriging, external drift kriging and index-based regionalisation) based on different combination of data types
251 (long series, short series, disaggregated daily series from weather radar parametrisation), while validating only on the
252 long and high-resolution observations. At the moment, a revision of the current design storm maps in Germany
253 (KOSTRA-DWD) is required in order to use additional data and state-of-the-art methodology. Therefore, an additional
254 aim of this study, is to give the basis for development of the new design storm maps in Germany (KOSTRA-2023).

255 The paper is structured as follows: first the available data sets for extreme value analysis are introduced in Section 2, then
256 the methods selected for investigation of the local and regional estimation are presented respectively in Section 3.1 and
257 3.2, with performance assessment and validation explained in Section 3.3. The results are given for each objective as:
258 best local estimation of extremes in Section 4.1, best regionalisation technique 4.2.1, best data integration 4.2.2. Finally,
259 the obtained maps for Germany are discussed in section 4.3 and conclusions are givendes in Section 5.

260 2. Study Area and Data

261 2.1 Available Data

262 The study area covers Germany and is illustrated in **Figure 1**Figure-1. Three rainfall measuring networks are
263 available from the German Weather Service (DWD); the daily **network-series** (DS) – typically Hellman devices recording
264 the rainfall daily, the long **network-series** (LS) – mostly tipping bucket analogue sensors (before 2004) measuring rainfall
265 at 1 min time steps with 0.1mm resolution and 2% uncertainty, and the most recent short **network-series** (SS) – digital
266 sensors (after 2004) measuring rainfall also at 1min timesteps with 0.01mm resolution. The spatial distribution of these
267 **networks-data series** is shown in **Figure 1**Figure-1, the observation length is given respectively in **Figure 2**Figure-2 and
268 the number of stations available for each **network-one** is given in **Table 1**Table-1. The **longLS dataset network** is the
269 most appropriate data set for extraction and evaluation of extreme rainfall statistics, since on average it includes 65 years
270 of observations (as shown in **Figure 2**Figure-2 – dark blue) and measures the rainfall at very fine temporal scales.
271 Nevertheless, this network is sparse **in comparison to the other two**, and only 133 stations in **the whole** Germany are
272 available. On the other side the **short-network-SS dataset** measures the rainfall as well at very fine temporal scales and is
273 much denser than the long **network-series** (1261 stations excluding the LS locations), however on average it includes only
274 18 years of observations which is not enough for extreme value **statistiesanalysis**. Lastly the **DS dataset daily-network** is
275 much denser (with 4068 stations excluding LS and SS locations) and covers 40 years up to 120 years, but the temporal
276 resolution of rainfall is too coarse to be useful for sub hourly extreme values analysis.

Formatted: Not Highlight

Formatted: Not Highlight

Formatted: Not Highlight

Formatted: Not Highlight

Formatted: Not Highlight

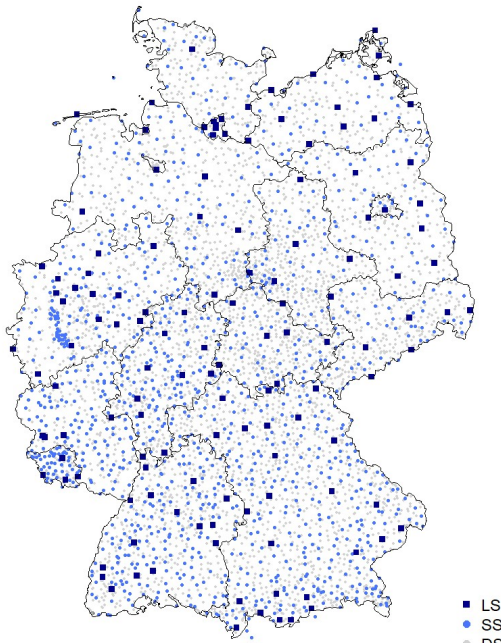


Figure 1 Available rainfall *networks-data types* in Germany for different temporal resolution. The black lines illustrate the borders of German Federal States.

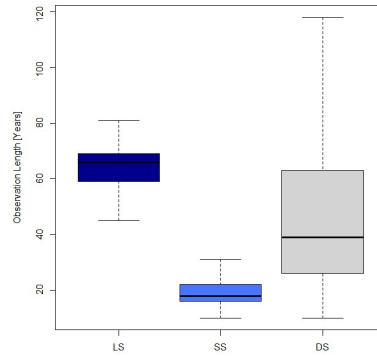


Figure 2 Observation length of all stations grouped according to the three available *networks-data types* in Germany.

Table 1 Number of stations for each of the available *networks-data types* in Germany.

Resolution	5min	1 day	
Obs. Length	> 41y	> 10 y	>10 y
No. Gauges	133	+1261	+4068

2.2 Temporal Disaggregation of the Daily *NetworkSeries*

The daily *network-dataset (DS)* is much denser than both long and short *networks-ones* and includes even longer observation periods than the *LS dataset/long-network*. If it is possible to disaggregate these data reliably, this will considerably increase the number of support points for the regionalisation of DDF curves. For the considerations presented here, the so-called cascade model first introduced by Olsson (1998) is employed. A more extensive parameterisation is implemented in the method according to Lisniak et al. (2013) which corresponds to a transfer of the Olsson method to a 3-fold distribution. To generate sub-hourly data, disaggregation parameters are derived from the RADOLAN *weather radar* time series of each grid cell (Bartels et al., 2004), and the daily observed volumes are disaggregated for the given durations as shown in **Table 2**. It is important to note that, due to the parameterisation using RADOLAN data, no parameter regionalisation is required, so that the parameter-rich disaggregation procedure in the Lisniak variant can be used. Moreover 30 realisations of disaggregated data were generated for each duration, in order to capture the uncertainty due to the disaggregation. It was evaluated that the relative error doesn't improve significantly for more than 30 realisations, as also reported in (Müller and Haberlandt (2018), therefore only 30 realisations of disaggregated data were used in this study.

Table 2 The disaggregation scheme applied to the daily *network-data (DS)* to obtain rainfall volumes at the given durations.

Duration	12h	8h	6h	4h	3h	2h	1h	30min	15min
----------	-----	----	----	----	----	----	----	-------	-------

Disaggregation 24h/2 24h/3 24h/2² 24h/3/2 24h/2³ 24h/3/2² 24h/3/2³ 24h/3/2⁴ 24h/3/2⁵

291 To understand what errors can be introduced to the DDF curves when employing this disaggregation scheme, a direct
 292 comparison was conducted between the long series (LS) and the disaggregated series (DS) for the return periods 1, 10,
 293 20, 50 and 100 years. For each station, duration level and return period, the relative error is calculated as the difference
 294 between the disaggregated and the original rainfall quantile. The resulting deviations for all stations are shown in **Figure**
 295 **3**. The results indicate that at the longer duration levels (>6 hours), the DDF curves are captured quite well, and
 296 the main disadvantage of the disaggregation model (as expected) is for the very short duration. Below the duration of 4
 297 hours, there is a clear tendency to underestimate the extremes **from LS, up to a median underestimation of 14% at the**
 298 **30min duration level. At the duration of 15min, a weakening of the underestimation is observed, which is probably due**

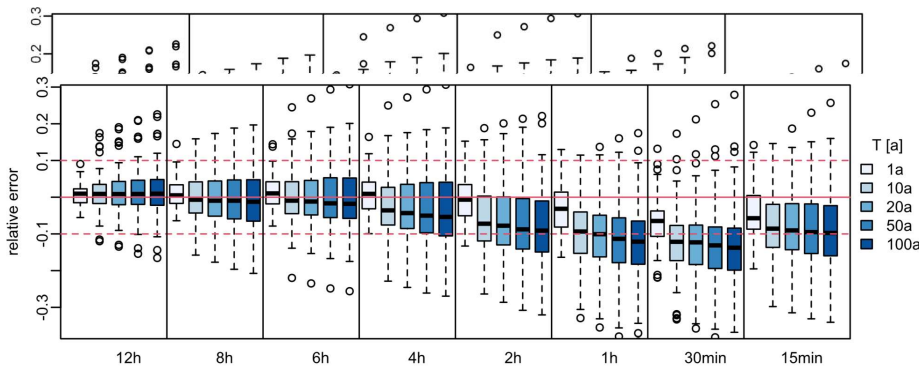


Figure 3 The relative error of the disaggregated daily station data (30 realisations) based on radar parametrisation for different return periods and duration levels: (+) sign indicates overestimation, while (-) sign underestimation of to the instationarity in the original series identified in Section 2.4 below, which predominates only at duration levels up to 15min. Thus, it is expected for the DS disaggregation scheme to be more useful for the longer duration extremes than the short ones. This is particularly true for the extremes at very short duration (5min) as the disaggregation scheme estimates volumes only down to 15 min durations: sub-hourly durations, where the extremes from DS are underestimated with more than 10% (not shown in).

- Formatted: Not Highlight
- Formatted: Not Highlight
- Formatted: Not Highlight
- Formatted: Not Highlight
- Formatted: Highlight
- Formatted: Font color: Text 1, Highlight

2.3 Annual Maximum Series for Each Dataset

305 Using the five-minute time series, annual maximum series (AMS) are derived based on the calendar year for the duration
 306 levels 5min, 10min, 15min, 30min, 1h, 2h, 6h, 12h, 1d, 2d, 3d and 7d. A moving window with the length of each duration
 307 level is used to derive the annual maxima, considering a dry duration of 4 hours to ensure that the maxima selected in
 308 December and January of two consecutive years are independent from one another. Additionally, following the guidelines
 309 given by DWA (2012) a scaling of the durations 5, 10 and 15 min AMS with the factors given in **Table 3** is
 310 performed. This is done to avoid the systematic underestimation of rainfall extremes at short duration caused by the
 311 deviation between i) the start of the actually largest rainfall sum of duration D, and ii) the fixed starting time of the 5 min
 312 time series (employed here).

Table 3 Correction factors for the short duration AMS according to the DWA-531(DWA, 2012).

Duration level	5min	10min	15min
Correction factor for AMS	1,14	1,07	1,04

2.4 Homogenisation of Long and Short Network Dataset

First plausibility and homogeneity checks were performed on the long and short data sets, herein referred to as respectively long series (LS) and short series (SS). An initial analysis of possible trends based on the quantile regression (Koenker, 2005) was carried out for the monthly 5min maximum intensities of the long series (LS). This method was chosen, as in comparison to the classical regression it is considerably more robust and it allows to obtain regression results for different non-exceedance probabilities. In Figure 4, the quantiles for the non-exceedance probabilities $\tau = 0.5$ (i.e. median), 0.8, 0.9 and 0.95 are considered. Quantile regressions for the four selected τ with time as the explanatory

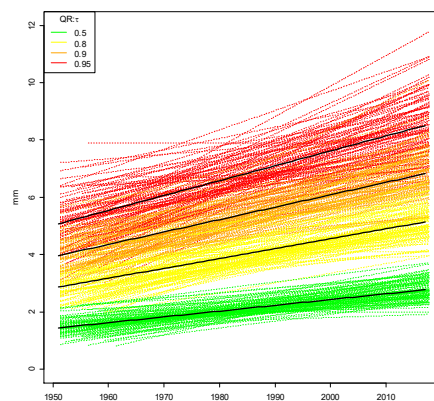


Figure 4 Quantile regression on monthly maximum 5 min rainfall intensities for the long series (LS) for different non-exceedance probabilities (shown in coloured dashed lines). The fitted quantile regression is shown with solid black line.

variable are implemented separately for each of the 133 measurement points. Each dashed line corresponds to a measuring station and each colour to a non-exceedance probability. Trend-like changes in the monthly five-minute maxima are visible with slopes that increase with τ . To understand why this trend is present in almost all long series, we investigated whether these instationarities are more trend-like or jump-like, with the latter assuming that the timing of jumps is associated with sensor changes in the measuring network. In the long network series, a total of 19 different sensor types are distinguished simply by two states: analogue or digital.

A test for trend, jump or stationarity based on in-stationary extreme value analysis (Coles, 2001) was performed for all 133 LS. We tested for linear trend in location parameter vs. jump at date of sensor change from analogue in early years to digital in the later years in the location parameter vs. stationarity. The decision was based on Akaike Information Criterion. The results for different duration levels (x-axis) are shown in Figure 5. It is obvious that the majority of instationarities at short duration levels is better explained as a jump (with mostly positive sign) in the data. A possible reason could lie in the limited ability of analogue gauges to register abrupt intensity changes, so that the total amount of precipitation falling in a short time interval may not be fully detected by analogue sensors, leading to positive jumps at sensor changes from analogue to digital. However, as a counter-argument, the so-called "step-response-error" that occurs with digital sensors could also be considered (see e.g. Licznar et al. (2015)). Since the instationarities are usually jumps and not trends, a simple homogenisation of the data to a uniform sensor type is possible by raising to the mean value of the digital sensor type (DVWK, 1999). This jump correction is applied separately for each station and duration level. The results of applying the instationarity test to the homogenised series are shown in Figure 5. It can be seen that this approach can eliminate the instationarities at short duration levels significantly. About 30%

Formatted: Not Highlight

339 of the stations show instationarities (either trend or jump), while the remaining part is considered stationary. Since only
 340 a small part of the stations show instationarities, here a stationary extreme value analysis is performed.

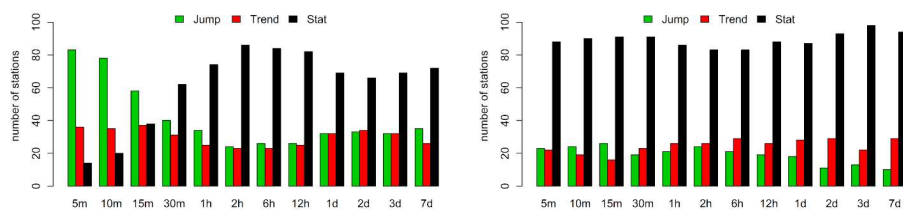


Figure 5 Trend vs Jump Analysis (%) for left) - before jump elimination, right) after jump elimination.

341 **3. Methods**

342 **3.1 Local Estimation of Extreme Value Statistics**

343 **3.1.1 Reference Approach**

344 Here, the Generalised Extreme Value (GEV) probability distribution is used for the statistical analysis of extreme
 345 rainfall and the derivation of the local DDF curves, that is described as following:

346
$$F(x; \mu, \sigma, \gamma) = \exp \left\{ - \left[1 + \gamma \frac{(x+\mu)}{\sigma} \right]^{-\frac{1}{\gamma}} \right\}, \quad 1 + \frac{\gamma(x-\mu)}{\sigma} > 0, \gamma \neq 0, \quad (1)$$

347 where μ is the location, σ the scale and γ the shape parameter. If the shape parameter is greater than zero, heavy-tail
 348 behaviour is present (GEV type II); if the shape parameter is less than zero, then it is the reverse Weibull distribution with
 349 no-tail behaviour (Coles, 2001). The GEV parameters are fitted to the AMS of each duration level and station separately,
 350 based on the L-moments method. For this purpose, the R-package “lmomco” was used (Asquith, 2021). A prior
 351 investigation on our study revealed that the L-moment approach led to more stable results than the method of Maximum
 352 Likelihood. The shape parameter was either estimated or fixed at 0.1 for estimation of return periods up to 100 years,
 353 approximately following the recommendation from Koutsoyiannis (2004a, b) [for estimation of return periods up to 100](#)
 354 [years \(\$\gamma=0.1\$ \)](#) and on a prior analysis conducted on [LSR](#) series. Based on the parameters obtained the quantiles of return
 355 periods T1a, T10a, T20a, T50a and T100a were derived. Since the AMS-approach tends to underestimate quantiles at low
 356 return periods ($T_a < 10$ years), a correction of the AMS return periods according to the DWA 531-Regulations with factors
 357 given in [Table 4](#) was performed.

Table 4 Correction of the Return Periods when fitting the GEV to the AMS adapted from (DWA, 2012).

Return Periods for POT	Ta=1 year	Ta=5 years	Ta=10 years
Return Periods for AMS	Ta=1.6 years	Ta=5.5 years	Ta=10.5 years

358 ~~As discussed previously in the introduction, b~~Because the parameters are fitted separately on each duration, quantile
 359 crossing may occur. [Quantile crossing happens when the extreme rainfall volumes of a fixed probability \(Ta=100 years\)](#)
 360 [are not increasing with longer duration levels.](#) [Figure 6](#) shows for different return periods T1a, T10a, T20a, T50a
 361 and T100a the number of stations affected by these crossings for the empirically calculated quantiles (left) and the
 362 quantiles fitted with the General Extreme Value (GEV) distribution (right). The empirical quantiles are calculated
 363 according to Hyndman and Fan (1996). It is clear that the number of stations with this problem increases significantly for
 364 larger return periods. In the empirical quantiles, especially the [short-series](#) show quantile crossing at the long duration
 365 levels ($D \geq 24h$). Here, the [extremes-volumes](#) of the duration-levels D72h and D168h are lower than the extremes of the
 366 [duration-level-D24h](#). With the GEV-fitted quantiles, significantly more stations show quantile crossings than with the

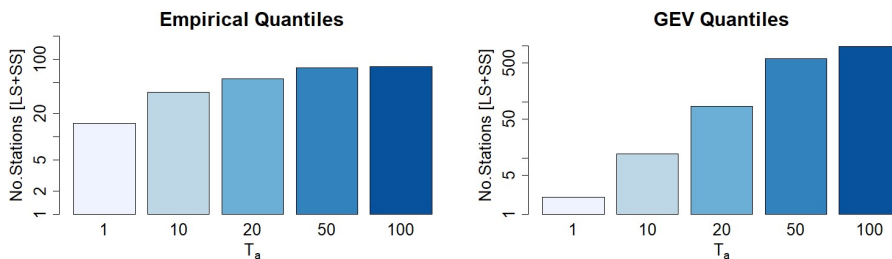


Figure 6 Number of stations for different return periods showing quantile crossings in the empirically calculated quantiles (left) and the GEV-fitted quantiles (right) with increasing duration.

367 empirically calculated quantiles. These problems occur for all return periods, however are more frequent for the return
368 periods T50a and T100a.

369 In order to avoid such problems two different methods are applied and compared here: the approach presented by
370 Koutsoyiannis et al. (1998) and the approach presented by Fischer and Schumann (2018). These two methods are
371 described below.

372 3.1.2 Koutsoyiannis Approach

373 Koutsoyiannis et al. (1998) considers the intensity as a function of the duration level through two parameters (θ, η) and
374 the generalised intensity can be calculated from duration specific intensity as described below:

$$375 \quad i = i_d \cdot b_d \quad \text{with } b_d = (d + \theta)^\eta, \quad (2)$$

376 where i is the generalised intensity in mm/h, i_d is the intensity in mm/h observed at each duration level, d is the duration
377 level in hours and θ, η are the Koutsoyiannis parameters optimised for each station. Through this relationship a
378 generalisation of the AMS intensities over all the chosen duration levels is possible. The parameters θ (larger than 0) and
379 η (within the range 0 to 1) are estimated for each station by minimising the Kruskal-Wallis statistic as indicated in
380 Koutsoyiannis et al. (1998). The advantage of this optimisation method lies in its non-parametric character and robustness,
381 as the Kruskal-Wallis statistics is not affected by the presence of extreme values in the sample. Once the parameters θ
382 and η are determined, the generalised intensities from all duration levels are pooled together (as the main assumption is
383 now that they follow the same distribution) and a GEV distribution is fitted to this sample by the methods of L-moments.
384 Lastly, to obtain DDF curves, the quantiles at specific return periods are estimated from the fitted GEV distribution, and
385 are divided by the term b_d in Equation (2) (dependable on θ, η parameters and the duration level). This joint estimation of
386 parameters over all durations should not only avoid the quantile crossings, but also make the estimation of DDF more
387 robust.

388 3.1.3 Fischer/Schumann Approach

389 In contrast to Koutsoyiannis that treats the intensities of AMS as a function of the duration, Fischer and Schumann (2018)
390 propose an ~~an~~ **new** approach based on the GEV distribution, where the generalised GEV parameters are monotonically
391 dependent on the GEV parameters determined for each duration level. Thus, as a first step the GEV parameters (as in
392 Equation (1)) are estimated from the L-moment methods for each duration level at each station, and then through a
393 nonlinear regression (with two parameters α and β) each GEV parameter is related to the different duration levels as
394 indicated by the following equations:

$$395 \quad \mu_d = \frac{\alpha_\mu}{d^{\beta_\mu}}, \quad \sigma_d = \frac{\alpha_\sigma}{d^{\beta_\sigma}} \quad \text{and} \quad \frac{\sigma}{\gamma} = \alpha + \beta \cdot d, \quad (3)$$

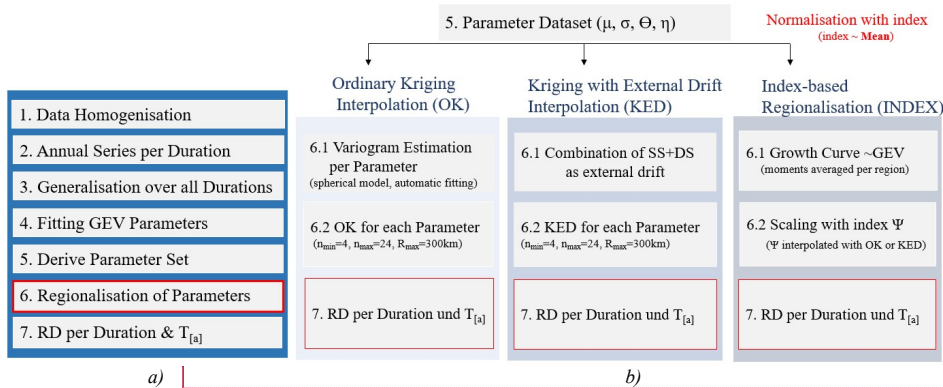
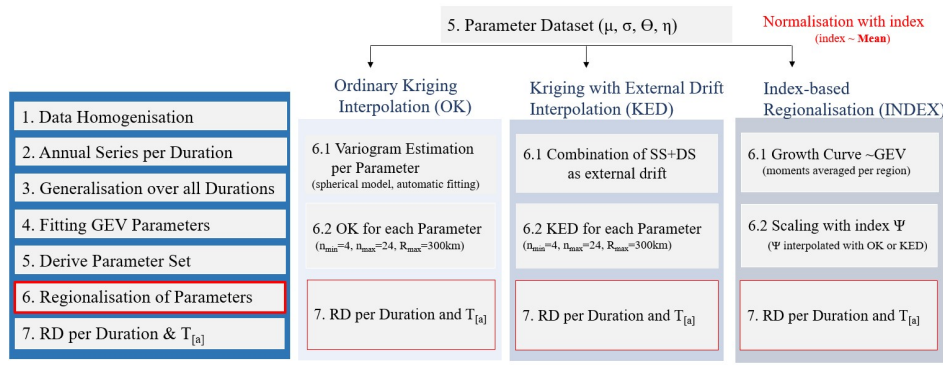
396 where d is the duration level in 5min, μ_d, σ_d, γ are the GEV parameters of each duration, while α and β are the regression
397 coefficients with $\alpha_\mu, \alpha_\sigma > 0, \beta_\mu, \beta_\sigma > -1, \beta \geq 0$. The parameters are obtained by nonlinear least-square-minimising. In
398 addition to the shape parameter dependency shown in Equation (3), three alternative approaches are considered: a constant
399 shape parameter over all durations, a shape parameter fixed at 0.1 and a quadratic relationship as in Equation (4).

$$400 \quad \xi = a + P_1 \cdot \log(d) + P_2 \cdot \log(d)^2, \quad (4)$$

401 where P_1 and P_2 are estimated spanning across all stations and a is a station specific optimised parameter.

402 3.2 Regionalisation of Extreme Value Statistics

403 The local parameters estimated for each station (GEV parameters and generalisation parameters) make the base data set
 404 for the regionalisation of the extreme rainfall statistics. Each of these parameters is regionalised independently based on
 405 the regionalisation methods explained below, and later on, DDF maps for each duration and return period of interest are
 406 generated. The overall procedure for regionalisation is given in **Figure 7** **Figure 7-a**, and the regionalisation methods are
 407 given in **Figure 7** **Figure 7-b**. The regionalisation approaches were compared only for 4 parameters (see parameters of
 408 **KO.FIX** in **Table 5**), as these 4 parameters were selected as most appropriate for local DDF estimation in **Section 4.1**.



410 **Figure 7 a)** Overall methodology from the given data sets to DDF maps for Germany, **b)** a short description of the regionalisation methods applied here only for the **KO.FIX** (see **Table 5**) local estimation of DDF; where RD is short for rainfall depth, and n_{min} , n_{max} and R_{max} are respectively the kriging parameters for minimum, maximum number of neighbours and maximum radius for neighbour search.

Commented [BS1]: I need to change the “und” to “and”

411 3.2.1 Ordinary Kriging Interpolation

412 The regionalisation of extreme value statistics for Germany will first be carried out with Ordinary Kriging (OK)
 413 interpolation. Here, the extreme rainfall parameters are interpolated independently. The flow chart for this interpolation
 414 technique is shown in **Figure 7** **Figure 7-b**. Ordinary Kriging is widely used for interpolation due to its simplicity in
 415 comparison to other kriging methods. The expected value of the random process being investigation (E) is treated as
 416 constant in space (as per Equation (5)), whereas the increase in variance of the target variable at any two location (u and
 417 $u+h$) depends only on the distance h . This increase in the variance is represented by the semi-variogram function $\gamma(h)$

14

(5)

(6)

418 (here called variogram). Therefore, in the first step, the empirical variogram is estimated by discrete point observations
 419 according to Equation (6).

420
$$E[Z(u+h)] = E[Z(u)] = m$$

421
$$\gamma(h) = \frac{1}{2N(h)} \sum_{u_i-u_j=h} (Z(u_i) - Z(u_j))^2,$$

422 where N is the number of any two observed data pairs (u_i and u_j) at distance h . Since the empirical variograms are not
 423 continuous functions, theoretical variograms must be fitted to the observed values. To describe the spatial variance of the
 424 data, several theoretical variogram models can be used and fitted to the empirical variogram using the least squares
 425 method. For the interpolation of rainfall extremes a spherical variogram (as per Equation (7)) is chosen as more
 426 appropriate (Kebaili Bargaoui and Chebbi, 2009).

427
$$\gamma(h) = c_0 + c \cdot \left(\frac{3h}{2a} - \frac{h^3}{2a^3}\right) \text{ for } h \leq a \text{ and } \gamma(h) = c \text{ for } h = a, \quad (7)$$

428 where c_0 is the nugget, c the sill and a the range of the variogram. The variogram describes the spatial variability of the
 429 target variable and the average dissimilarity between a known and unknown location. Once the theoretical variogram is
 430 known, it can be used as a basis for interpolating the statistical properties on a $5\text{km} \times \text{m}^2$ -grid. This grid resolution was
 431 chosen for two reasons: first it is consistent with the HyRas product from German Weather Service that uses the same
 432 resolution, second it is a compromise between the coarsest and finest legible resolution computed from the given density
 433 of long series (LS) (the reference for this study) following the suggestions of (Hengl, (2006). Here the interpolation is
 434 done, as indicated in Equation (8), the variable at an unknown location (Z') is estimated by the weighted average of the
 435 nearby known locations (Z_{u_i}).

436
$$Z'(u_0) = \sum_{i=1}^n \lambda_i \cdot Z(u_i), \quad (8)$$

437 where the weights (λ_i) are derived from the theoretical variogram, and n is the number of selected neighbours. The R-
 438 package "gstat" is used to fit the variograms and interpolate the variables (Pebesma, 2004). An advantage of Ordinary
 439 Kriging interpolation is that the weights are determined in such a way that the difference between the estimate and the
 440 observed values is zero on average. However, this can lead to the interpolated variable being smoothed in space.

441
 442 Different theoretical variograms were previously investigated, i.e. exponential, gaussian and spherical, with the spherical
 443 model together with a nugget effect showing the best fit for the case study. The fitting of the variogram model parameters
 444 for different data types and experiments is done automatically by weighted least square fit. Since the automatic fit relies
 445 on the initial values of the model parameters, we defined the initial values with trial and error, and accepted a fit that was
 446 adequate qualitatively. Figure 8 illustrates the empirical and theoretical normalised variograms for interpolation of the
 447 GEV and Koutsoyiannis parameters (after method KO.FIX shown in Table 5), estimated from the three main datasets
 448 available: long series (LS), short series (SS) and 30 realisations of disaggregated daily series (DS). Note that the
 449 variograms are normalised in order to ensure a comparison between the different datasets. From this figure a clear
 450 difference between the spatial dependency of different datasets, due to different station densities and settings, is visible.

Formatted: Not Highlight
 Formatted: Not Highlight
 Formatted: Not Highlight
 Formatted: Not Highlight
 Formatted: Not Highlight

Formatted: Font color: Text 1
 Formatted: Font color: Text 1

Formatted: Font color: Text 1
 Formatted: Font color: Text 1
 Formatted: Font color: Text 1
 Formatted: Font color: Text 1
 Formatted: Font color: Text 1
 Formatted: Font color: Text 1

Formatted: Font: Bold
 Formatted: Caption, Left, Space After: 0 pt, Border:
 Top: (No border), Bottom: (No border), Left: (No
 border), Right: (No border), Between : (No border)

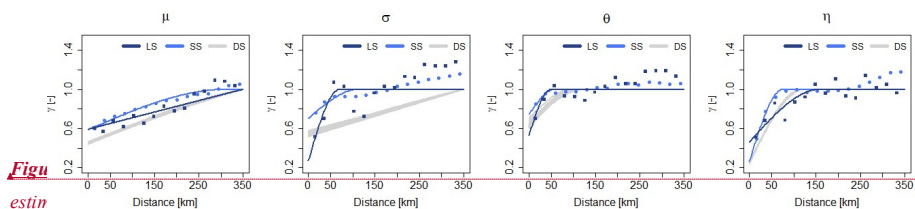


Fig 8
 estin

The long and short series (LS and SS) exhibits similar relationship with each other for the GEV parameters (μ and σ) but distinguish either in the nugget value (c_0) or the range (a), whilst the daily disaggregated series clearly exhibit different nugget (c_0), range (a) and even sill (c). The differences between the datasets are less visible in the spatial dependencies of the Koutsoyiannis parameters (θ and μ), where the three datasets differ slightly in nugget and range. Particularly the spatial dependency of the scale parameter is captured quite differently by the three datasets. Here, LS and SS are differing mainly at the nugget value, where LS has a smaller value than the SS series suggesting that the spatial structure of the scale parameter from SS is smoother than that of LS. On the other hand, the DS datasets exhibit a completely different variogram for the scale parameter, suggesting that the extremes of high return period (influenced mainly by the scale parameter) will have different spatial structures than those of LS and SS series.

Formatted: Font color: Text 1

3.2.2. Kriging with External Drift Interpolation

In the Kriging with External Drift (KED), the expected value E of the target variable Z at any location u is linear dependent on secondary variables Y , and thus the Equation (5) takes the form of the Equation (9). Here the secondary variables (or the external drifts) reflect the spatial trend of the target variable. Theoretically, the variogram for KED interpolation is computed from the residuals between the target and the secondary variables. Here, for simplicity the OK variograms are used instead, since as shown in (Delrieu et al., (2014) Delrieu et al. (2014)) they can produce very similar results to the KED one.

Field Code Changed

$$E[Z(u) | Y_1(u), Y_2(u), \dots, Y_m(u)] = b_0 + \sum_{k=1}^m b_k Y_k(u) \quad (9)$$

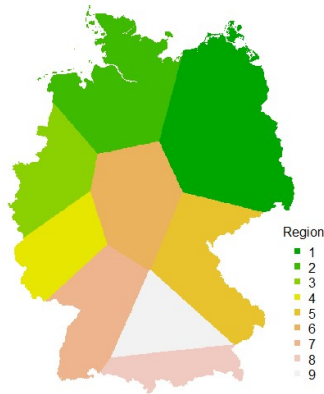
where Y represent the k secondary variables from 1 to m that is used as an external drift, and b_0 in the interception of the linear dependency and b_k the coefficient for each k drift. For this study different site characteristics (i.e. elevation) were investigated as external drift, however as indicated by the cross-correlation between the target variables (in this case the 4 parameters describing the local statistics) and the site characteristics, the linear dependency between them is not high (see in appendix Figure A1). Therefore, here only interpolated local parameters from the short and/or daily network series are used as external drift information.

3.2.3 Index-based Regionalisation

The regionalisation of extreme rainfall statistics in Germany is as well carried out using the index method according to Hosking and Wallis (1997). The index method was originally developed for the regionalisation of flood quantiles, however found a wide application also for the regionalisation of extreme rainfall statistics. By pooling information in statistically homogeneous regions, a more robust estimate of extreme rainfall statistics can be made and on the basis of the regions the information based on each defined region, the information can be transferred to other unobserved points. A homogeneous region exists if the distribution functions have the same shape at all points in the region. The homogeneity indicator H_1 presented by Hosking and Wallis (1997) is typically used to determine homogeneous regions. If the H_1 is lower than 1, the region is said to be homogeneous, if it is between 1 and 2 the region may be heterogeneous, and else, if it is higher than 2, the region is definitely not homogeneous. Here different site characteristics like the latitude, longitude, elevation, long term annual average of sunshine duration and mean annual precipitation were used as input to define homogeneous regions. Based on a k-clustering approach (Ward, 1963) 9 homogeneous regions were identified and are shown in Figure 9 Figure 8. The obtained homogeneous regions were tested for homogeneity for each data type combination and, as visible from Figure A2 in appendix, all values are below 1, meaning that the regions selected are homogeneous and can be used for the index-based regionalisation. Note that the generalised statistics over all the durations from Section 3.1 are used as input for the homogeneity test. The R-package "nsRFA" is used to obtain the homogeneous regions (Viglione et al., 2020). In order to find an appropriate number of clusters, different number of clusters between 2

491 [and 20 are tested and compared based on the homogeneity indicator H1 and whether they were spatially continuous and](#)
 492 [physically reasonable. The maximum number of clusters of 20 was chosen to ensure a sufficient number of stations and](#)
 493 [thus a sufficient number of observation years per region \(Hosking and Wallis, 1997\).](#)

494 Once the homogeneous regions are determined, the different local statistics are normalised by a scaling factor, the index.
 495 In contrast to the previous regionalisation techniques discussed so far, the index-based regionalisation has an extra step –
 496 the normalisation of the general intensities with the index [\(performed at step 3 in Figure 7 – left\)](#), which in this case is
 497 the mean generalised intensity. Next, the local L-moments are estimated on the basis of the normalised annual series and
 498 regional L-moments are derived for each region weighting the local L-moments according to their time series length.
 499 Finally, a GEV growth curve is fitted for each region [and duration-level](#) via the regional L-moments. The R-package
 500 “lmomRFA” was employed for the application of the index method (Hosking and Wallis, 1997). In the final step, by
 501 back-scaling the normalised extreme rainfall for all observed and unobserved points in the homogeneous region, estimates
 502 can be made about the extreme rainfall as a function of the duration [\(based on regional averaged values of observed \$\theta\$ and](#)
 503 [\$\eta\$ \)](#) and the return period [\(based on regional GEV growth curve\)](#). The geostatistical interpolation of the index makes it
 504 possible to transfer the extreme value statistical evaluations to unobserved points within the region.



505 **Figure 98** Nine homogeneous regions implemented here for the index-based regionalisation. The regions shown here
 are a generalisation of the k -cluster results to account for spatial consistency.

506 **3.3 Performance Assessment and Comparison**

507 **3.3.1 Local Performance Assessment**

508 For the local estimation of the GEV parameters that describe the extreme rainfall over all the selected duration levels, two
 509 different approaches were consulted: from Koutsoyiannis et al. (1998) (herein referred as KO) and from Fischer and
 510 Schumann (2018) (herein referred as FS). Before carrying on with the regionalisation it is important to investigate which
 511 of the methods is more adequate for the estimation of the GEV parameters over all the duration levels. Moreover, the two
 512 methods do not only distinguish in their approach of generalisation across duration, but they also include different
 513 variations on the calculation of the [GEV-shape GEV-parameter \(\$\gamma\$ \)](#). A review of the methods and shape parameters is
 514 given in [Table 5](#)[Table 5](#), together with the respective optimised parameter set for each case. The obtained parameters for
 515 different data sets are shown in the appendix: [Figure A3](#) for KO and in [Figure A4](#) for FS.

Table 5 A review of the methods and the different calculation of the shape parameter investigated for the local statistics.

Method	Shape Parameter	Abbreviation	Optimised Parameter
	is constant per each station, as fitted by L-moments	KO.CON	$\mu, \sigma, \gamma, \theta, \eta$

KO	is fixed at all stations as $\gamma = 0.1$	KO.FIX	$\mu, \sigma, \theta, \eta$
FS	is calculated as proposed by Fischer and Schumann	FS.RLM	$\alpha_\mu, \beta_\mu, \alpha_\sigma, \beta_\sigma, \alpha, \beta$
	is constant over all durations	FS.CON	$\alpha_\mu, \beta_\mu, \alpha_\sigma, \beta_\sigma, \gamma$
	a quadratic dependence on duration specific shape	FS.QUA	$\alpha_\mu, \beta_\mu, \alpha_\sigma, \beta_\sigma, a$
	is fixed at all stations as $\gamma = 0.1$	FS.FIX	$\alpha_\mu, \beta_\mu, \alpha_\sigma, \beta_\sigma$

516 The performance of the methods and the respective case of shape parameters as illustrated in **Table 5Table 5** is evaluated
517 only at the location of the long series (LS) by comparing the normalised quantiles over all durations for return periods
518 T1a, T10a, T20a, T50a and T100a with the GEV quantiles calculated separately at each duration level. Here the percentage
519 RMSE (as per Equation (10)) was employed to assess the errors of the selected cases at each duration level and station
520 with respect to the GEV duration specific quantiles:

$$521 \quad \text{Percentage RMSE:} \quad RMSE_{d,st}[\%] = 100 \cdot \frac{\sqrt{\frac{1}{5} \sum_{i=1}^5 (RD_{gen,st} - RD_{d,st})^2}}{\overline{RD}_{d,st}}, \quad (10)$$

522 where i represents each of the 5 selected return period T_a varying from 1 to 100 years, st varies from 1 to 133 available
523 long series, $RD_{gen,st}$ corresponds to the derived rainfall depth from the generalisation method of duration d , $RD_{d,st}$ the
524 derived rainfall depth from the GEV quantiles at duration d , and the $\overline{RD}_{d,st}$ is the mean rainfall depth from the GEV
525 quantiles at a duration d averaged over the return periods. Alternatively, the error for each return period and station can
526 as well be calculated by Equation (10) by swapping the d with T_a , and where $\overline{RD}_{T_a,st}$ is the mean rainfall depth from the
527 GEV quantiles at return period T_a averaged over the duration levels d (from 5min up to 7d, therefore i changes from 1 to
528 12).

529 Since the GEV quantiles fitted per each duration level cannot be considered the ground truth, a non-parametric bootstrap
530 is performed when estimating the parameters of each method, in order to investigate the sampling uncertainty of derived
531 DDF values. For this purpose, 100 randomisations of the observations were conducted and the uncertainty range of the
532 derived rainfall depths is computed as following:

$$533 \quad \text{Normalised 95\% Confidence Interval Width:} \quad nCI95_{width}, nCI95[-] = 100 \frac{CI95_{st,d,Ta}}{Mean_{st,d,Ta}} \quad (11)$$

534 where $nCI95_{width}$ is the 95% confidence interval width and Mean is the average of rainfall depth obtained from 100
535 realisations and expressed for each LS location st , duration level d and return period T_a . The smaller the uncertainty range,
536 the more robust are the estimated parameters for the high return periods. Based on the two performance criteria, percentage
537 RMSE and $nCI95_{width}$, all the methods in **Table 5Table 5** are compared in order to evaluate the best one for the estimation
538 of rainfall DDF curves. The best method is selected as the one with the lowest RMSE and $nCI95_{width}$. The results of this
539 comparison are given in Section 4.1.

540 3.3.2 Spatial Performance Assessment

541 In order to check which of the regionalisation approaches provides the best results, a leave-one out cross-validation was
542 carried out at the locations of the long series (LS 133 stations). For each approach, the rainfall depth (RD) is determined
543 from the return periods T1a, T10a, T20a, T50a and T100a and the selected duration levels. After regionalisation, the
544 regionalised rainfall depths are compared with the local generalised GEV quantiles (here assumed to be the truth). The
545 short series are omitted from the cross-validation, as no reliable extreme value statistics can be carried out for large return
546 periods due to the very short observation length. The quality of the regionalisation approaches is evaluated using the
547 following criteria:

Formatted: Font: Italic

Formatted: Subscript

548 Percentage Bias:
$$PBIAS_{st,Ta} [\%] = 100 \cdot \frac{\frac{1}{D} \sum_{d=1}^D (RD_{regional,d} - RD_{local,d})}{\sum_{d=1}^D (RD_{local,d})}, \quad (12)$$

549 Percentage RMSE:
$$RMSE_{st,Ta} [\%] = 100 \cdot \frac{\sqrt{\frac{1}{D} \sum_{d=1}^D (RD_{regional,d} - RD_{local,d})^2}}{RD_{local}}, \quad (13)$$

550 Nash-Sutcliffe Criteria:
$$NSC_{st,Ta} [-] = 1 - \frac{\sum_{d=1}^D (RD_{regional,d} - RD_{local,d})^2}{\sum_{d=1}^D (RD_{local,d} - \overline{RD_{local}})^2}, \quad (14)$$

551 where the d is the selected duration level varies from 1 to $D=12$ for each duration level between 5min and 7days, T_a the
 552 return period, st the respective LS, $RD_{regional}$ corresponds to the regionalised rainfall depth, RD_{local} the locally derived
 553 rainfall depth from the ~~normalised-generalised~~ GEV function and the $\overline{RD_{local}}$ $\overline{RD_{local}}$ is the mean local rainfall depth
 554 averaged over the 133 locations. The cross-validation only at the location of the LS makes it possible to investigate the
 555 value that the short (SS) and the disaggregated daily ~~network-series~~ (DS) are adding to each regionalisation method. For
 556 this purpose, the regionalisation methods are run first only with the LS as input, and the performance of such an application
 557 is considered the benchmark for improvement. Later on, the SS and DS are added stepwise as input to the regionalisation,
 558 in order to assess the improvement, they introduce towards the benchmark. Additionally, one can calculate the expected
 559 performance when only the short or/and the disaggregated daily ~~networks-series~~ are available, and not the ~~automatic-long~~
 560 one. An overview of these experiments and their aim is given at ~~Table 6~~ ~~Table 6~~.

Table 6 Overview of the experiments performed with different data sets for each regionalisation method.

Input	Aim
Only LS	Benchmark for improvement
Only SS	The expected error from only short networkseries
Only DS	The expected error from only disaggregated daily networkseries
LS and SS	The added value from the short networkseries
LS and DS	The added value from the daily disaggregated networkseries
SS and DS	The expected error from short and daily disaggregated series daily-network
LS, SS and DS	The added value from the short and daily disaggregated series daily-network

561 A directed comparison of the performance criteria between the different experiments and the benchmark is calculated
 562 here as per Equation (15).

563
$$Perf_{impr,Ta} [\%] = 100 \cdot \frac{(-Perf_{new,Ta} + Perf_{ref,Ta})}{Perf_{ref,Ta}}, \quad (15)$$

564 where $Perf_{ref,Ta}$ is the performance criteria calculated for each return period Ta as per Equation (12)-(14) from the scenario
 565 with only LS as input, and $Perf_{new,Ta}$ is the performance of any other combination of input data as per Equation (12)-(14).
 566 A positive value for this criterion indicates an improvement in performance in comparison to the only LS scenario, while
 567 a negative value indicates a deterioration. Note that, the signs of the nominator are exchanged in the case of the
 568 improvement of the NSE. It is as well important to emphasise that the scenario ref corresponds to the best regionalisation
 569 method with only LS as input, namely ordinary kriging of LS based on results of Section 4.2.

570 Finally, based on different combinations of the available ~~network-series (data types)~~ as external drift in the kriging
 571 interpolation may help to shed light on which combination of the data is more useful for the regionalisation of the rainfall
 572 DDF values. Here the data to be used as external drift are first interpolated with ordinary kriging (also in cross-validation
 573 mode). A description of these different combinations for the KED interpolation is given is ~~Table 7~~ ~~Table 7~~. The

- Formatted: Italian (Italy)
- Formatted: Italian (Italy)
- Formatted: Italian (Italy)
- Formatted: Italian (Italy)
- Formatted: Italian (Italy)
- Formatted: Italian (Italy)
- Formatted: Italian (Italy)
- Formatted: Italian (Italy)
- Formatted: Italian (Italy)
- Formatted: Italian (Italy)
- Formatted: Italian (Italy)
- Formatted: Italian (Italy)
- Formatted: Italian (Italy)
- Formatted: Italian (Italy)
- Formatted: Italian (Italy)
- Formatted: Italian (Italy)

574 performance of the different combinations is evaluated only at the location of the LS, and the best integration is selected
575 based on the highest improvement in comparison to regionalisation with only LS as input.

Table 7 Overview of different integration of data types in the interpolation with KED. Pooling the data together with same importance is represented by (+) sign, whereas integration through an external drift (linear dependence) is represented by the (|) sign.

Combination	Abbreviation
Interpolate LS with OK[SS] as external drift	KED[LS SS]
Interpolate LS with OK[DS] as external drift	KED[LS DS]
Interpolate LS with both OK[SS] and OK[DS] as external drift	KED[LS SS+DS]
Interpolate LS and SS with OK[DS] as external drift	KED[LS+SS DS]
Interpolate SS with OK[DS] as external drift	KED[SS DS]

576

577 4. Results

578 4.1 Local Estimation of Extreme Statistics

579 **Figure 10** **Figure-9** illustrates the local percentage RMSE of each method in comparison to the duration specific quantiles
580 (as per Equation (10)). The upper row of **Figure 10** **Figure-9** shows the percentage RMSE calculated for each location
581 and duration level over all the return periods and the lower row of **Figure 10** **Figure-9** shows the percentage RMSE
582 calculated for each location and return period over all the duration levels. The results from **Figure 10** **Figure-9** – upper
583 row indicate that the KO approaches (both fix and station constant shape parameter) have an almost constant RMSE over
584 all durations under the value 10%. On the other hand, the FS approaches tend to have similar or little smaller RMSE for
585 the longer duration (median RMSE under 8%), but are not able to represent well enough the very short durations. For the
586 FS approaches, the RMSE median for duration levels up to 60 min, is higher than 10%, with the 5min RMSE being the
587 highest (between 25-45%). The results from **Figure 10** **Figure-9** – lower row illustrate that all the approaches manifest
588 higher errors with higher return period. Both of the KO approaches (fix and station constant shape) show very similar
589 behaviour. The KO.FIX performs slightly worse (1-4% higher RMSE) than the KO.CON, but this is expected as the
590 duration GEV fitted per each duration independently favours the KO.CON (as the shape parameter is let free for the GEV
591 parameter fitting). The FS approaches perform very similarly to one another, however here contrary to the KO.FIX
592 approach, the performance of the FS.FIX seems better than the other approaches. Overall, the KO approaches have the
593 priority at shorter durations and they can capture the volumes at specific durations better than the FS approaches. On the
594 other side, the FS approaches can capture better extremes at longer durations. A unanimous selection is not yet possible
595 from the obtained results so far, because the local GEV duration specific parameters may not represent the ground truth.

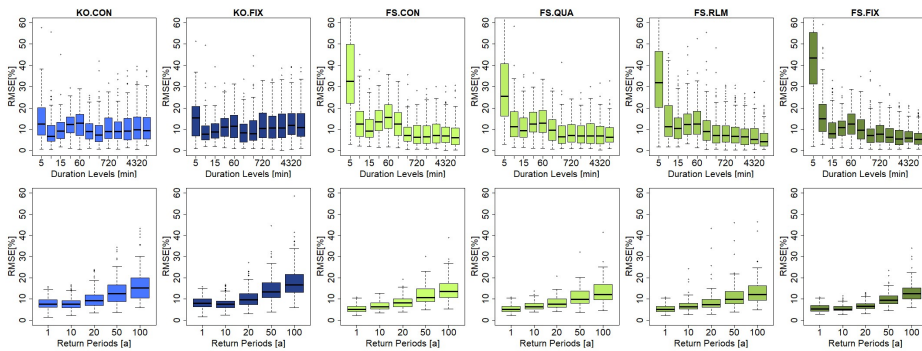
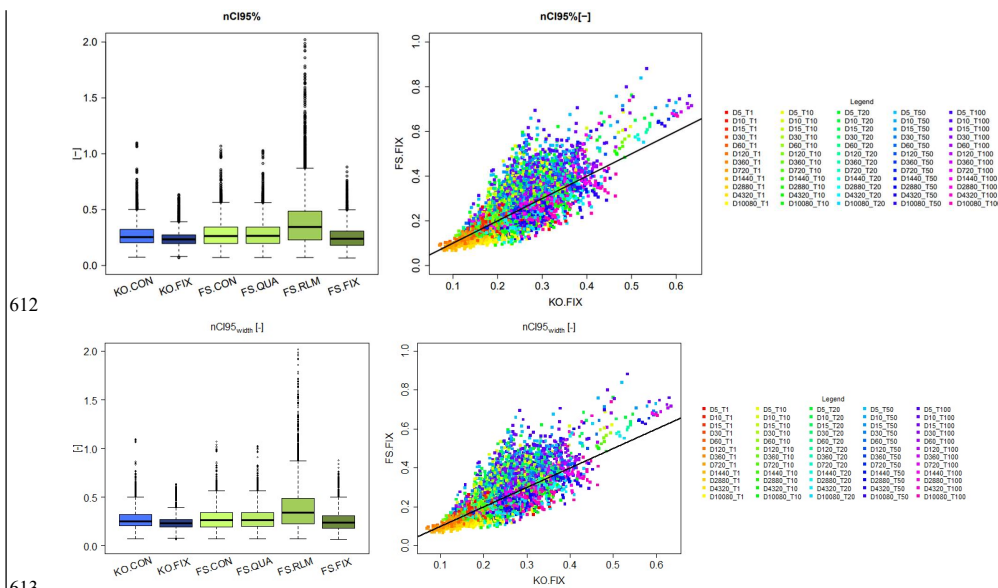


Figure 109 RMSE (%) performance of the given generalisation methods over all the long stations (LS) in comparison to the duration specific GEV quantiles grouped: upper row - for different duration levels (calculated per station over return periods), and lower row - for different return periods (calculated per station over duration levels).

596 To analyse which approach estimates more stable and representative parameters, a non-parametric bootstrap was
597 performed (with 100 random realisations), and served as a basis for assessing the 95% confidence interval *width* of the
598 obtained DDF values. **Figure 11** **Figure-10**-left shows the normalised 95% confidence interval *width* (nCI_{95}^{width}) for
599 the rainfall depth (as per Equation (11)) estimated for each of the selected approaches. A high value of the nCI_{95}^{width}
600 indicates that the bootstrap yields very variable rainfall depths, and hence a higher uncertainty is associated with the
601 method. Contrarily a low value of the nCI_{95}^{width} indicates that the rainfall depths have low variation across the random
602 realisations, and thus the obtained DDF curves are considered more stable or robust. The results shown in **Figure**
603 **11** **Figure-10** indicate that the KO.FIX exhibits the lowest variation (median $nCI_{95}^{width} \sim 0.23$), followed up by FS.FIX

604 (~0.25), and by KO.CON, FS.CON, FS.QUA with slightly higher variations (respectively ~0.3). Interesting is to see that
 605 the FS.RLM has a median $nCI95_{width} \sim 0.3$, but can reach extreme values up to 2. **Figure 11** **Figure 10**-right) shows the
 606 scatterplot of $nCI95_{width}$ obtained from the KO.FIX (x-axis) and FS.FIX (y-axis) for different duration levels and return
 607 periods (shown with different colours) at the LS locations. Except for very low return periods (T1a), FS.FIX exhibits on
 608 average higher values of $nCI95_{width}$ than KO.FIX. Based on these results, the KO.FIX was chosen as the best method and
 609 was used for the regionalisation of the DDF curves. The advantages of the KO.FIX are that: 1. It represents all duration
 610 levels similarly and fairly, 2. The parameter estimation is more robust than any of the other methods, 3. It uses a known
 611 and well-established method for the estimation of the DDF curves.



612 **Figure 11** **10** left) comparison of confidence interval robustness for the methods and shape parameters selected for the
 613 generalisation of the DDF values over all the durations; right) a direct comparison of the confidence interval robustness
 for KO.FIX (x-axis) with FS.FIX (y-axis) for each duration and return period (shown in different colours).

614 4.2 Regionalisation of Extreme Statistics

615 As discussed in the Section 4.1, the AMS at different duration levels were normalised according to Koutsoyiannis
 616 approach and the GEV parameters were fitted to the grouped generalised intensities. The shape parameter was kept fixed
 617 at 0.1. Ordinary Kriging (OK) and index-based (INDEX) regionalisation were run first only with the LR data as input –
 618 to decide about which of the two approaches will serve as a benchmark. A direct comparison based on Equation (15) is
 619 then performed for each of the selected performance criteria (where *new* is OK and *ref* is INDEX), to compute the
 620 improvement or deterioration of OK with only LS data compared to the INDEX. The median values for each return period,
 621 performance criteria and method, are given in **Table 8** **Table 8**. Here it becomes clear that the kriging approach exhibits
 622 lower RMSE for all return periods, worse BIAS for high return periods, and slightly better NSE than the index method.
 623 Based on these results, the kriging with LS as input (KRIGE[LS]) is used as a benchmark for calculating the improvement
 624 in performance by adding additional data types. Apart from the performance, the other advantage of kriging is that, it is
 625 more of a “pure” method, as it interpolates independently the 4 parameters, while the index approach is a “mixture”

626 between the regional growth curve estimation, averaging θ and η parameters, and kriging to interpolate the index. For this
 627 reason, one may prefer the kriging regionalisation, as the errors are mainly from the kriging system, while the index
 628 method includes errors from the kriging system and from regional and averaged parameters.

Table 8 Median performance improvement/deterioration (%) of ordinary kriging (OK) versus index-based (INDEX) interpolated calculated for different data as per Equation (15) (where new is OK and ref in INDEX), when only LS dataset is used as input. The performance is obtained by cross-validation over 133 LS stations. The colour green (+) indicates better performance by OK, red (-) indicates better performance by INDEX.

	RMSE (%)					PBIAS (%)					NSE (%)				
	T1a	T10a	T20a	T50a	T100a	T1a	T10a	T20a	T50a	T100a	T1a	T10a	T20a	T50a	T100a
LS	5.270	1.230	-0.268	0.015	1.510	2.500	-1.200	-1.440	-3.440	-2.469	0.250	0.010	0.002	0.002	0.006

629

630 4.2.1 Best Regionalisation for Different Data Combination

631 Kriging and index-based regionalisation was then performed for each data type experiment given in **Table 6**, and
 632 the cross-validation results for the 133 LS locations were compared to the benchmark (KRIGE[LS]) selected before as
 633 the best regionalisation with only LS as input. To enable an easy comparison between the two regionalisation methods,
 634 the difference between the improvements achieved between the kriging and the index-based regionalisation in comparison
 635 to the benchmark was calculated for each of the 133 LS locations. The median differences (in percent) for each data type
 636 experiment over the 133 locations for each performance criteria and return period are given in **Table 9**. A positive
 637 difference (dark green shade) means that the improvements reached by the kriging interpolation are higher than the index-
 638 based regionalisation. A negative difference (red shade) means *vice-versa*. The data are combined by two
 639 operators: either (+) referring to pooling of the datasets together and the parameters and the index are interpolated with
 640 ordinary kriging, and (|) referring to a linear relationship between the datasets and the parameters and the index are
 641 interpolated through external drift kriging.

Table 9 Median difference between kriging and index-based improvements calculated for different data as per Equation (15). The median is computed from 133 stations. The positive difference shown in green shades indicate that kriging introduces bigger improvements towards the benchmark than the index-based regionalisation. The negative differences shown in red shades indicate that the index-based regionalisation has the bigger improvements.

	RMSE (%)					PBIAS (%)					NSE (%)				
	T1a	T10a	T20a	T50a	T100a	T1a	T10a	T20a	T50a	T100a	T1a	T10a	T20a	T50a	T100a
SS	15.1	8.2	9.6	-0.1	0.4	6.5	10.4	4.8	1.5	-2.3	-0.1	0.6	0.0	0.0	-0.1
DS	19.4	4.8	6.1	10.1	12.2	-2.6	2.9	8.0	11.5	11.8	0.4	0.3	0.8	0.8	0.9
LS+SS	8.3	3.6	6.4	-2.3	-0.8	8.0	3.5	0.2	-6.7	-11.4	0.3	0.2	0.2	0.2	-0.1
LS SS	5.5	11.6	12.3	9.8	10.8	13.0	8.6	3.6	6.1	6.0	0.2	0.3	0.5	0.5	0.5
LS+DS	101.2	90.4	75.3	77.3	76.9	157.5	162.9	154.7	134.1	130.5	10.1	10.0	10.1	10.1	10.0
LS DS	20.7	16.6	16.1	15.5	12.8	27.6	12.6	10.5	3.9	1.4	0.7	0.4	0.4	0.4	0.3
SS+DS	111.0	97.5	82.5	79.0	82.6	176.0	194.6	188.7	157.2	150.8	10.3	9.8	9.8	9.8	9.4
SS DS	10.6	6.8	8.8	4.0	5.1	9.9	-3.4	-2.8	-2.3	-5.9	0.2	0.4	0.3	0.3	0.2
LS+SS+DS	59.8	44.1	45.5	43.3	41.4	110.4	132.6	141.8	109.7	107.3	5.1	4.6	4.4	4.4	4.1
LS+SS DS	13.1	12.2	13.2	10.6	11.9	10.4	2.0	-0.8	1.0	-2.8	0.2	0.5	0.5	0.5	0.5
LS SS+DS	20.1	13.3	11.5	6.1	3.3	18.2	8.1	8.1	-0.2	-1.9	0.5	0.3	0.2	0.2	0.1

642

643 The results from the **Table 9** indicate that for the majority of the cases the kriging interpolation brings higher
 644 improvements to the benchmark than the index-based regionalisation. Exception are the regionalisation with only SS,
 645 LS+SS, SS|DS, LS+SS|DS and LS|SS+DS where the index-based regionalisation exhibits on median 2-12% higher
 646 PBIAS improvement for higher return periods than the kriging interpolation. However, for these cases, the RMSE and
 647 the NSE improvements are much higher for the kriging regionalisation. Therefore, it can be concluded that overall the

648 kriging interpolation yields better results than the index-based regionalisation (lower RMSE and higher NSE), but may
 649 suffer depending on the combination of data types from slightly higher PBIAS.- Also, it has to be mentioned, that when
 650 grouping the daily disaggregated time series directly (operator +) with the other data types (either LS and SS), the kriging
 651 performs up to 100% better than the index-based regionalisation. This suggests that the parameters from the
 652 disaggregation do not follow the same regions or growth curve as the high-resolution data (LS and SS), thus a kriging
 653 interpolation seems to be more reasonable ~~when for~~ including these data as well.

654 The results of ~~Table 9~~ **Table 9** give a direct comparison between kriging and index-based regionalisation, nevertheless as
 655 they are relative to each case, do not give any information if ordinary kriging or external drift kriging is yielding better
 656 regionalisation results. For this purpose, the difference of improvements between KED and OK were calculated and
 657 shown as median over the 133 LS locations in ~~Table 10~~ **Table 10**. A positive difference (green shade) means that the
 658 improvements reached by KED are higher than the OK interpolation. A negative difference (red shade) means otherwise.
 659 The results show that overall the KED exhibits higher RMSE and NSE improvements than the OK, but the KED tends to
 660 have lower PBIAS improvements than the OK. When only the high-resolution data sets are present (LS and SS), the KED
 661 behaves better than OK mainly for high return periods (50-100a), when LS and DS are present, KED clearly outperforms
 662 the OK. For all the remaining cases the OK outperforms the KED only for the PBIAS of high return periods.

Table 10 Median difference between external drift kriging (KED) and ordinary kriging (OK) improvements calculated for different data as per Equation (15). The median is computed from 133 stations. The positive difference shown in green shades indicate that KED introduces bigger improvements towards the benchmark than the OK. The negative differences shown in red shades indicate that the OK regionalisation has the bigger improvements.

	RMSE (%)					PBIAS (%)					NSE (%)				
	T1a	T10a	T20a	T50a	T100a	T1a	T10a	T20a	T50a	T100a	T1a	T10a	T20a	T50a	T100a
LS and SS	-6.4	2.0	-1.9	7.8	8.8	-1.3	-4.9	-5.2	1.2	6.2	-0.5	-0.2	0.1	0.1	0.5
LS and DS	56.4	41.0	39.4	32.9	30.2	57.6	30.5	20.7	14.5	13.2	2.5	1.7	1.6	1.6	1.5
SS and DS	46.4	30.5	27.2	26.3	27.8	37.1	1.0	-8.1	-11.3	-14.9	1.9	1.4	1.3	1.3	1.4
LS+SS DS	42.2	20.2	19.7	17.4	20.2	39.3	-0.5	-16.0	-18.6	-19.9	1.8	1.2	1.0	1.0	1.2
LS SS+DS	40.0	20.6	16.3	16.4	16.4	37.0	-2.5	-21.5	-16.8	-17.7	1.6	1.0	0.9	0.9	1.0

664 4.2.2 Best Data Integration for Regionalisation

665 So far, the external drift kriging interpolation has shown superiority for regionalising DDF curves in comparison to the
 666 index-based and ordinary kriging regionalisation. Nevertheless, the question still remains, what is the best combination
 667 of the data sets for regionalising the DDF curves in Germany. Here it is interesting to see if all the three available data
 668 sets are useful for regionalisation, or if single or dual networks are enough. For this purpose, the performance
 669 improvement exhibited by different combinations of the data types in KED (as per ~~Table 7~~ **Table 7**) in comparison to the
 670 benchmark are visualised in ~~Figure 12~~ **Figure 11**. Note that since there are 30 realisation of DS data, a boxplot is
 671 illustrating the performance spread over these 30 realisations. This affects regionalisation methods where DS data is
 672 present, otherwise a ~~horizontal-single~~ line indicates the performance of the regionalisation. For very low return periods
 673 (T1a), the integration of all data types of the form KED[LS+SS|DS] brings the best performance, with RMSE and BIAS
 674 up to 20% smaller and NSE 0.7% higher. For return period T10a, the KED[LS|SS], KD[LS|DS] and KED[LS+SS|DS]
 675 perform very similar: some random realisation from the disaggregated daily network (DS) introduce high improvement
 676 but as well low values, even though the median over the 30 realisation is at the same level as the KED[LS|SS] one. For
 677 high return periods (T100a), KED[LS|SS] introduces the highest improvement in all three performance criteria. Actually
 678 KED[LS|DS] is the second-best option, however the median over the 30 realisations is either lower or equal to the
 679 performance of the KED[LS|SS]. There are few realisations that introduce the highest improvements for RMSE and BIAS,
 680 nevertheless the computation time for the disaggregation scheme and the fitting of the Koutsoyiannis approach is also a

681 disadvantage of using the DS data type. So finally, the kriging interpolation of the long network (LS) with the short
 682 network (SS) as an external drift, is chosen as an optimal method for the regionalisation of the GEV and Koutsoyiannis
 683 parameters. **Table 11** indicates the median performance criteria (RMSE, PBIAS, NSE) for different return
 684 periods reached by this method (KED[LS/SS]). **Expected deterioration in performance when the long series are not present**
 685 **in comparison to the best method selected for regionalisation (KED[LS/SS]) are given in Figure A5 in the appendix.**

686 **Table 11** Median cross-validation performance over 133 stations for the final selected regionalisation method.

	T1a	T10a	T20a	T50a	T100a
KED[LS/SS]					
RMSE (%)	8.11	8.06	8.24	8.46	8.86
PBIAS (%)	1.00	1.10	0.80	1.00	0.80
NSE (-)	0.982	0.981	0.979	0.979	0.980

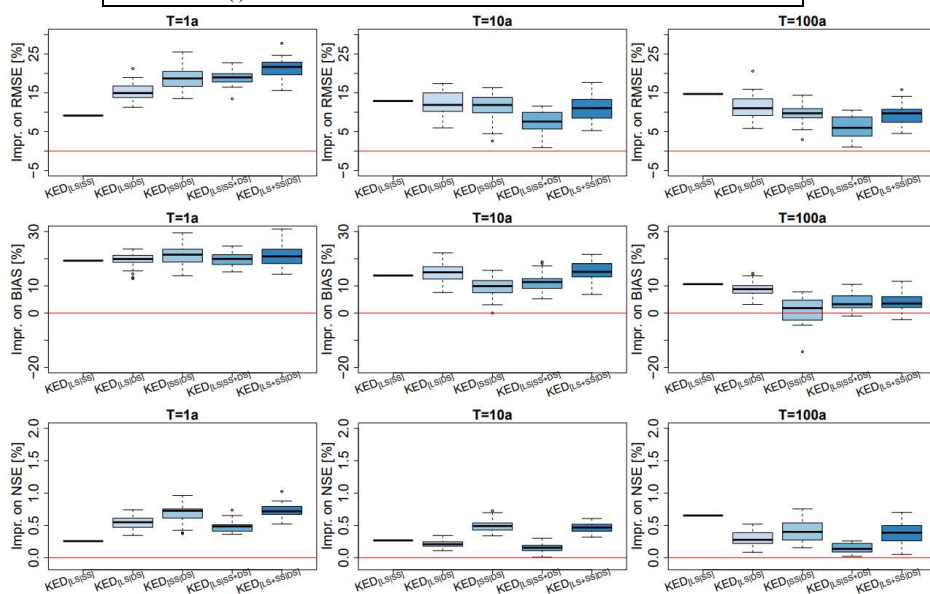


Figure 124 Median performance improvements towards the benchmark from regionalising on different data combinations, as per **Table 7**, in kriging with external drift.

687 **The three different data sets implemented here, distinguish from one another based on the parameter values (as shown in**
 688 **Figure A3 of the appendix) also on the spatial dependency, variograms, shown in Figure 8. When fixing the shape**
 689 **parameter to 0.1, the location and Koutsoyiannis parameters of LS and SS, are in similar range, and the main difference**
 690 **is seen at the scale parameter (where the SS has high values of the scale parameter than LS). This gives a tendency of the**
 691 **short durations to estimate bigger rainfall volumes for higher return periods. This behaviour is also in agreement reported**
 692 **by Madsen et al. (2017), which used a Generalised Pareto distribution also with a fix shape parameter. Typically, this is**
 693 **treated by index-based regionalisation, where extremes within a region are pooled together to estimate the DDF curves at**
 694 **an unknown location as done in Requena et al. (2019). However, we show here that integrating the LS and SS with**
 695 **external drift kriging, hence accounting for the spatial dependency of the extremes, delivers better performance than**
 696 **grouping them together in the index-based regionalisation (also valid for the LS and DS integration).**

Formatted: Font: Not Italic

Formatted: Not Highlight

Formatted: Font: Bold

Formatted: Font color: Auto

Formatted: Font: Bold, Font color: Auto

Formatted: Font color: Auto

Formatted: Font color: Auto

Formatted: Font color: Auto

Formatted: Font color: Auto

Formatted: Font color: Auto

Formatted: Font color: Auto

Formatted: Font color: Auto

697 **4.3 Final Product and Discussion**
698 -The obtained maps, on a 5 by 5 km raster, for the four regionalised parameters (location parameter μ , scale
699 parameter σ , Koutsoyiannis θ and η parameters) with the KED[LS]SS approach, are illustrated in **Figure 13**
700 Here the shape parameter is fixed to 0.1 for whole Germany, which is very similar to results obtained by (Ulrich et al.,
701 (2021), (shape parameter as 0.11 from the annual GEV approach) and validates our approach. The spatial distribution of
702 the location GEV parameter (μ) follows partly the elevation information, with higher values in the south east, where the
703 German Alps are located. The scale GEV parameter (σ) values are independent of the elevation, with a high localised
704 value near to Münster city. Recently in 2014, there was has been a very extreme event in Münster which has affected the
705 statistics of the station located in the vicinity. Currently it is not clear how to handle these singular extraordinary events
706 in extreme value analysis in an optimal way. Both Koutsoyiannis parameters (θ and η) show similar spatial patterns with
707 lower values in the Alp and other mountainous regions, as well as on the northern-west coast. These parameters exhibit
708 higher variability in space than the GEV location or scale parameters. Overall, the spatial distribution of η parameter
709 follows the spatial structure of the annual rainfall sum in Germany, the distribution of the location (μ) parameter follows
710 the information from the elevation, while the scale (σ) and θ parameter don't seem to be influenced by any climatologic
711 or site characteristic. This is also seen at (Van De Vyver (-2012), where annual rainfall and elevation is concluded as
712 important covariates, mainly for the location (μ) parameter, while the scale (σ) parameter didn't have meaningful
713 covariates and the shape parameter didn't show any spatial structure but was kept constant over Belgium. These results
714 agree to a certain extend with the results obtained here. However, the rainfall statistics extracted from short or daily series
715 are considered as more important than the annual rainfall (which itself is an interpolation from point observation). Thus,

Formatted: Font color: Auto

Formatted: Font color: Auto

Formatted: Font color: Auto

Formatted: Font color: Auto

Formatted: Font color: Auto

Formatted: Font color: Auto

Formatted: Font color: Auto

716 interpolation of long datasets, should include extreme statistics from short or daily series rather than annual rainfall as an
 717 additional information. With these 4 interpolated maps, together with the shape parameter fixed at 0.1, DDF curves can
 718 be obtained for any location in Germany. Few examples of design rainfall maps for duration levels 5min, 1 hour and 1
 719 day, and return period $T_a=1,10,100$ years, are given in Figure 13. For short durations (i.e. $D=5$ min) the spatial
 720 distribution of rainfall extremes is independent from the elevation and becomes more erratic with higher return periods.
 721 This is in accordance with the fact that the convective extreme events can happen anywhere and are very low correlated
 722 with the orography. With increasing duration level, the relationship between orography and extreme rainfall becomes
 723 stronger. As for instance in $D=1h$, the influence of the alpine regions is visible, which becomes even stronger for the
 724 duration of $D=1d$.

Formatted: Font color: Auto

Formatted: Font color: Auto

Formatted: Font color: Auto

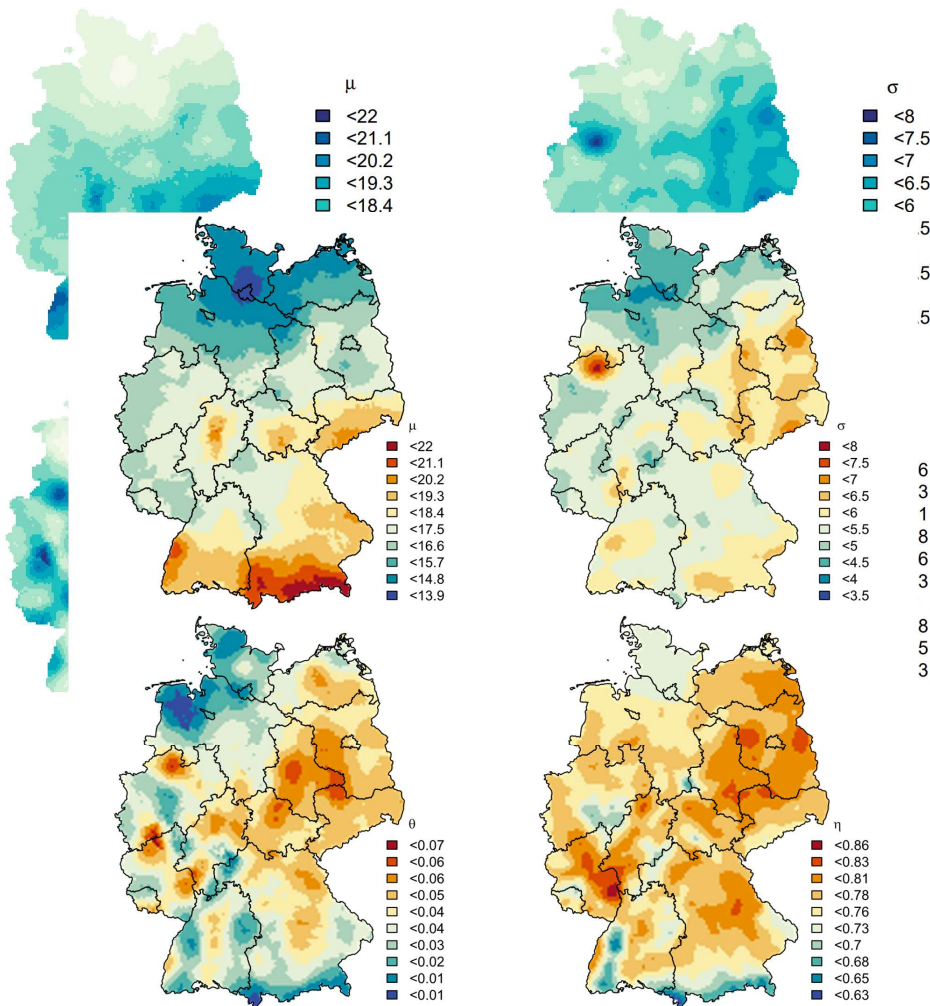


Figure 13.2 Obtained interpolated maps from the KED[LS|SS] for each of the parameter: location parameter - μ , scale parameter - σ , Koutsoyiannis θ and η parameters. The shape parameter γ is kept constant at 0.1.

725

726 With these 4 interpolated maps, together with the shape parameter fixed at 0.1, DDF curves can be obtained for any
727 location in Germany. Few examples of design rainfall maps for duration levels 5min, 1 hour and 1 day, and return period
728 $T_a=1,10,100$ years, are given in **Figure 14**. For short durations (i.e. $D=5$ min) the spatial distribution of rainfall extremes
729 is independent from the elevation and becomes more erratic with higher return periods. This is in accordance with the
730 fact that the convective extreme events can happen anywhere and are very low correlated with the orography. With
731 increasing duration level, the relationship between orography and extreme rainfall becomes stronger. As for instance in
732 $D=1h$, the influence of the alpine regions is visible, which becomes even stronger for the duration of $D=1d$. In the existing
733 KOSTRA maps, all durations are dependent on elevation. Here, the elevation itself didn't show much effect on the scale
734 (σ) and θ parameter, only to some extent on the location (μ) and η parameter. This means that the extremes of longer
735 duration (affected by the η parameter) and of low return period (affected by the location parameter) will show a pattern
736 resembling the elevation. This is not true for short durations (affected by the θ parameter) and high return periods (affected
737 by the scale parameter). This as well agrees with other studies, that report a weak dependence of short duration rainfall
738 (shorter than 1 or 2 hours) with the elevation in Germany (Lengfeld et al., 2019). Lastly, the kriging interpolation as
739 implemented here, opens the possibility to capture better the uncertainty – not only the sample uncertainty which is
740 typically done by bootstrapping the points statistics, but accounting as well the spatial structure of extremes by considering
741 spatial simulations. This results in estimates that will be more precise near to the location of long time series, and less
742 precise in regions far from long time series (Shehu and Haberlandt, 2022).

Formatted: Font color: Auto

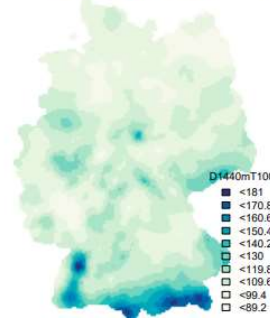
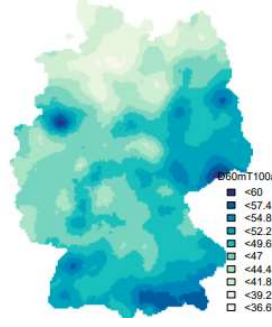
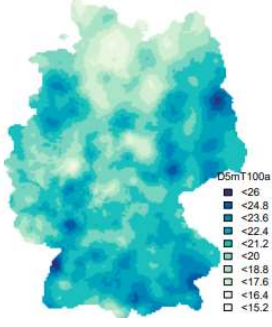
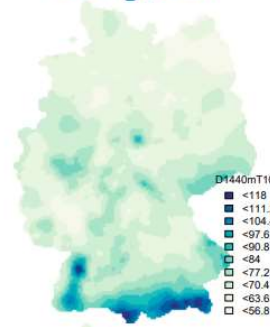
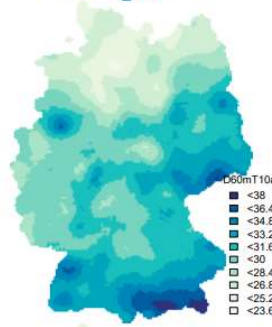
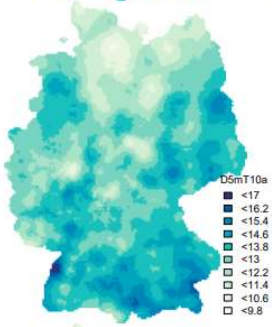
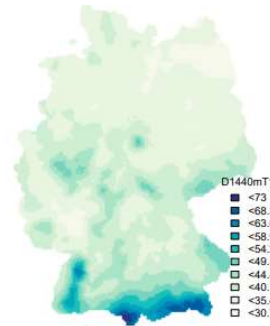
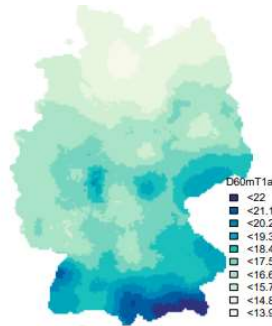
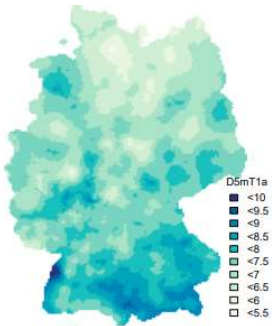
Formatted: Font color: Auto

Formatted: Not Highlight

Formatted: Font color: Auto

Field Code Changed

Formatted: Font: Not Italic, Font color: Dark Blue



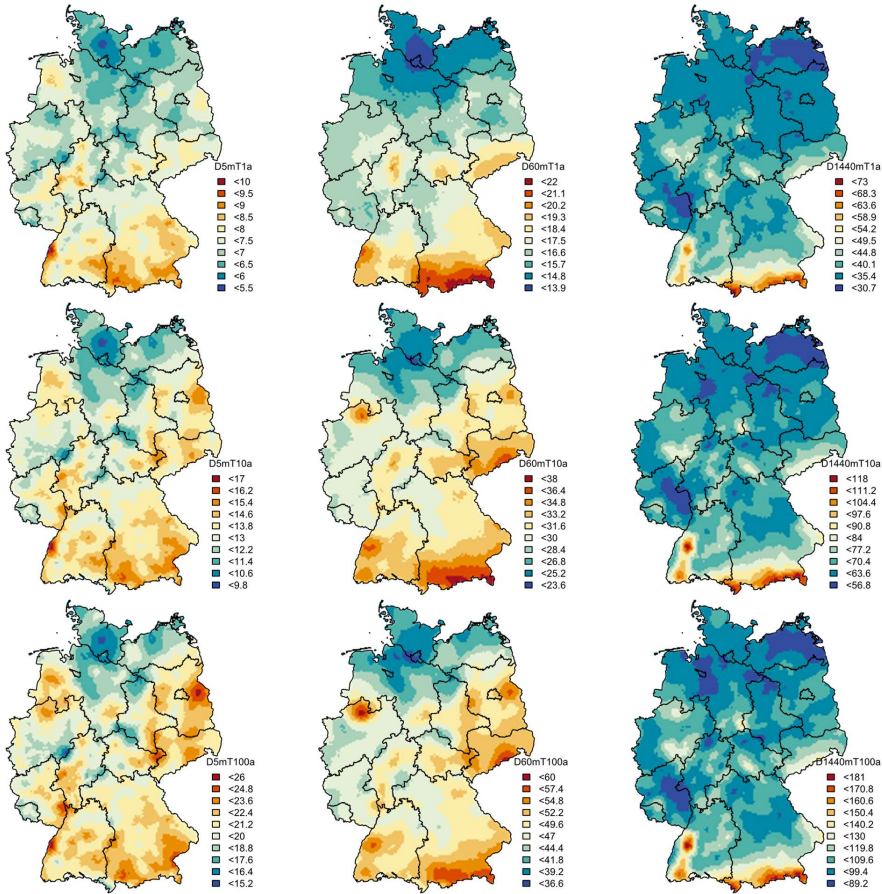


Figure 1413 Obtained design rainfall [mm] maps for whole Germany from the KED[LS|SS] regionalisation approach derived for different durations: first row – return period $T_a=1$ -year, second row – return period $T_a=10$ years and third row – return period $T_a=100$ years.

746 **5. Conclusions**

747 In this study the use of three ground measuring **networks-types** in Germany was investigated for the estimation of design
748 rainfall maps. These **networks-data types** included the long high-resolution **networkdataset**, with long observations at 5
749 min time steps from 60-70 years, the short high-resolution **network-dataset** with short observation also at 5 min time steps
750 from 10 to 20 years, and the daily **network-dataset** with observations varying from 20 to 100 years. The purpose of the
751 work was to review different methods for the estimation and regionalisation of the DDF curves and to investigate the
752 value and the best integration of different data types for estimating DDF curves in **ungauged-unobserved** locations. The
753 results will provide the basis for a new update of the design storm maps for Germany, the KOSTRA-DWD2023. First,
754 the long **analogous** and **short-recent digital** high-resolution networks were homogenised by performing a jump correction,
755 with the jumps coinciding with sensor type changes. Second the daily **network-dataset** was disaggregated to sub hourly
756 durations based on a cascade model parameterised according to Olsson, (1998) and Lisniak et al. (2013) from the
757 RADOLAN data in Germany. Third, Annual Maximum Series (AMS) were derived for each station available in the three
758 **networks-datasets** for duration levels ranging from 5 min to 7 days. This represents the main database for the present
759 investigation. Two methods were investigated for local estimation of rainfall extreme statistics, adopted from
760 Koutsoyiannis et al. (1998), and Fischer and Schumann (2018), and three different regionalisation approaches (ordinary
761 kriging, external drift kriging and index-based regionalisation) were investigated for the spatial estimation of DDF curves
762 in Germany. The conclusions derived, by considering the long high-resolution **network-dataset** as the truth, are
763 summarised as:

- 764 • Both methods for local estimation of the rainfall extreme statistics behave quite similarly in capturing the
765 local duration specific rainfall depths.
- 766 • Nevertheless, the estimation of parameters through the Koutsoyiannis approach is more robust in terms
767 of data sampling uncertainties. Particularly the Koutsoyiannis approach combined with a Generalised
768 Extreme Value (GEV) distribution with a fixed shape parameter value at 0.1 exhibited the highest
769 robustness with tolerable decline in precision. Therefore, 4 parameters were used to describe the local
770 statistics of extreme rainfall: the location and scale GEV parameters and the two Koutsoyiannis
771 parameters θ and η . These 4 parameters represent the basis for the testing of different scenarios and
772 regionalisation approaches.
- 773 • When only the long high-resolution **network-dataset** is present, both ordinary kriging and index-based
774 regionalisation perform similarly, with ordinary kriging showing slightly better median performance.
775 This result remains true as well for other data combination settings, with kriging methods exhibiting lower
776 RMSE and NSE, but slightly higher PBIAS than the index-based regionalisation. The only case where
777 the index-based regionalisation has slight superiority against kriging, is when only short high-resolution
778 series are present.
- 779 • When more than two **networks-datatypes** are available, kriging with external drift seems more adequate
780 for the parameter interpolation than ordinary kriging, at least regarding the RMSE and NSE
781 performance.
- 782 • A combination of long and short **networks-high resolution series** improves the performance of
783 regionalisation considerably (up to 15% for $T_a=100$ years), but only when the data sets are combined
784 with external drift kriging. Here the **digital-parameters from the short series are network-is** first
785 interpolated with ordinary kriging, which later on, serves as an external drift for the kriging interpolation

of the parameters from the long network series. This combination gave overall the best results at least for return periods higher than 10 years.

- A combination of the long high-resolution and daily networks-dataset improves the performance of regionalisation up to 10% being the second-best method for regionalisation. Here as well the best regionalisation was the external drift kriging, with the ordinary kriging interpolation of daily network parameters serving as an external drift.
- A combination of the three networks-data types improves the regionalisation considerably (up to 20%) only for low return periods (shorter or equal than 10 years).
- Overall, the best method for the regionalisation of the DDF curves in Germany, was the kriging interpolation of the long sub hourly stations, with the short sub hourly stations as an external drift. On average, this approach exhibited 8-9% RMSE (increasing with the return period) and up to 1% BIAS (decreasing with the return period) when compared to the locally estimated DDF curves.

The cross-validation implemented here can only describe the accuracy of the regionalisation methods when compared to the local estimation, but it does not say much about the precision of the predictions. Thus, it is important to perform an uncertainty analysis, which should include not only the local estimation of sample statistics (briefly discussed here) but as well the spatial uncertainty of the kriging interpolation. An investigation is currently going on for the integration of spatial uncertainty in the DDF design storms of Germany, as discussed in Shehu and Haberlandt (2022). Further improvements of the methodology, might include the validation of the methods on distinguished region. It has to be noted that the majority of the reference stations in Germany are located in the lowlands, thus the mountainous areas may be under-represented. It would be interesting to investigate if daily data or other site characteristics (like the elevation) are improving the performance of the chosen method in these regions. However, should one decide to perform region specific regionalisation, special care should be paid to the continuity of DDF values at the borders of the regions. Lastly, these conclusions are valid mainly for Germany, where dense networks are present. The advantage of each data set or approach may still change depending on the station density or study area location.

6. Data Availability

The daily and the short sub-daily network are made publicly available by the German Weather Service (DWD) and can be accessed at https://opendata.dwd.de/climate_environment/CDC/. The long sub-daily network has been digitalised and provided by the DWD. All R-codes can be provided by the corresponding authors upon request.

7. Authors Contribution

Supervision and funding for this research were acquired by UH and WW, the study conception, design and methodology were performed by all authors, while the software, data collection, derivation and interpretation of results were handled mainly by BS and WW (with support of the other authors). BS prepared the original draft, which is revised by all authors.

8. Competing Interest

The authors declare that they have no conflict of interest.

9. Funding

This research was funded by the German Ministry of Agriculture and Environment Mecklenburg-Vorpommern and the Federal State Funding Programme "Water, Soil and Waste".

Formatted: Font: 10 pt, Font color: Black, English (United Kingdom)

Formatted: Not Highlight

823 **10. Acknowledgements**

824 The results presented in this study are part of the research project "Investigating Different Methods for Revising and
825 Updating the Heavy Rainfall Statistics in Germany (MUNSTAR)", funded by the German Ministry of Agriculture and
826 Environment Mecklenburg-Vorpommern and the Federal State Funding Programme "Water, Soil and Waste" who are
827 gratefully acknowledged. We are also thankful for the provision and right to use the data from the German National
828 Weather Service (Deutscher Wetterdienst DWD), more specific Thomas Deutschländer and Thomas Junghänel.

829 **11. References**

- 830 Asquith, W. H.: Lmomco: L-moments, censored L-moments, trimmed L-moments, L-comoments, and many
831 distributions., 2021.
- 832 Bara, M., Kohnová, S., Gaál, L., Szolgay, J. and Hlavčová, K.: Estimation of IDF curves of extreme rainfall by simple
833 Scaling in Slovakia, *Contrib. to Geophys. Geod.*, 39(3), 2009.
- 834 Bárdossy, A. and Pegram, G.: Combination of radar and daily precipitation data to estimate meaningful sub-daily point
835 precipitation extremes, *J. Hydrol.*, 544, 397–406, doi:10.1016/J.JHYDROL.2016.11.039, 2017.
- 836 Bartels, H., Weigl, E., Reich, T., Lang, P., Wagner, A., Kohler, O., Gerlach, N. and MeteoSolutions GmbH: Projekt
837 RADOLAN - Routineverfahren zur Online-Aneicherung der Radarniederschlagsdaten mit Hilfe von automatischen
838 Bodenniederschlagsstationen (Ombrometer), Offenbach am Main., 2004.
- 839 Berndt, C., Rabiei, E. and Haberlandt, U.: Geostatistical merging of rain gauge and radar data for high temporal
840 resolutions and various station density scenarios, *J. Hydrol.*, 508, 88–101, doi:10.1016/j.jhydrol.2013.10.028, 2014.
- 841 Borga, M., Vezzani, C. and Fontana, G. D.: Regional Rainfall Depth-Duration-Frequency Equations for an Alpine
842 Region, *Nat. Hazards*, 36, 221–235, 2005.
- 843 Burn, D. H.: A framework for regional estimation of intensity-duration-frequency (IDF) curves, *Hydrol. Process.*,
844 28(14), doi:10.1002/hyp.10231, 2014.
- 845 Cannon, A. J.: Non-crossing nonlinear regression quantiles by monotone composite quantile regression neural network,
846 with application to rainfall extremes, *Stoch. Environ. Res. Risk Assess.*, 32(11), doi:10.1007/s00477-018-1573-6, 2018.
- 847 Ceresetti, D., Ursu, E., Carreau, J., Anquetin, S., Creutin, J. D., Gardes, L., Girard, S. and Molinié, G.: Evaluation of
848 classical spatial-analysis schemes of extreme rainfall, *Nat. Hazards Earth Syst. Sci.*, 12(11), 3229–3240,
849 doi:10.5194/nhess-12-3229-2012, 2012.
- 850 Coles, S.: *An Introduction to Statistical Modeling of Extreme.*, 2001.
- 851 Delrieu, G., Wijbrans, A., Boudevillain, B., Faure, D., Bonnifait, L. and Kirstetter, P. E.: Geostatistical radar–raingauge
852 merging: A novel method for the quantification of rain estimation accuracy, *Adv. Water Resour.*, 71, 110–124,
853 doi:10.1016/J.ADVWATRES.2014.06.005, 2014.
- 854 Durrans, S. R. and Kirby, J. T.: Regionalization of extreme precipitation estimates for the Alabama rainfall atlas, *J.*
855 *Hydrol.*, 295(1–4), doi:10.1016/j.jhydrol.2004.02.021, 2004.
- 856 DVWK: *Statistische Analyse von Hochwasserabflüssen*, Merkblatt 251, Bonn, 62 S, 1999.
- 857 DWA: *Arbeitsblatt DWA-A 531: Starkregen in Abhängigkeit von Wiederkehrzeit und Dauer*, DWA Arbeitsgruppe HW
858 1.1e, Hennef, Deutschland., 2012.
- 859 Fischer, S. and Schumann, A. H.: Berücksichtigung von Starkregen in der Niederschlagsstatistik, *Hydrol. und*
860 *Wasserbewirtschaftung*, 62(4), 221–240, doi:10.5675/HyWa, 2018.
- 861 Forestieri, A., Lo Conti, F., Blenkinsop, S., Cannarozzo, M., Fowler, H. J. and Noto, L. V.: Regional frequency analysis
862 of extreme rainfall in Sicily (Italy), *Int. J. Climatol.*, 38(January), e698–e716, doi:10.1002/joc.5400, 2018.
- 863 Goudenhoofd, E., Delobbe, L. and Willems, P.: Regional frequency analysis of extreme rainfall in Belgium based on
864 radar estimates, *Hydrol. Earth Syst. Sci.*, 21(10), doi:10.5194/hess-21-5385-2017, 2017.

Formatted: German (Germany)

Formatted: German (Germany)

865 Gupta, V. K. and Waymire, E.: Multiscaling properties of spatial rainfall and river flow distributions, *J. Geophys. Res.*,
866 95(D3), 1999–2009, doi:10.1029/JD095iD03p01999, 1990.

867 Hengl, T.: Finding the right pixel size, *Comput. Geosci.*, 32(9), 1283–1298, doi:10.1016/j.cageo.2005.11.008, 2006.

868 Holešovský, J., Fusek, M., Blachut, V. and Michálek, J.: Comparison of precipitation extremes estimation using
869 parametric and nonparametric methods, *Hydrol. Sci. J.*, 61(13), doi:10.1080/02626667.2015.1111517, 2016.

870 Hosking, J. R. M. and Wallis, J. R.: *Regional Frequency Analysis*, Cambridge University Press., 1997.

871 Hyndman, R. J. and Fan, Y.: Sample Quantiles in Statistical Packages, *Am. Stat.*, 50(4), 361–365,
872 doi:10.1080/00031305.1996.10473566, 1996.

873 Johnson, F. and Sharma, A.: Design Rainfall, in *Handbook of Applied Hydrology*, edited by V. P. Singh, pp. 125–3 to
874 125–13, McGraw-Hill, New York., 2017.

875 Kebaili Bargaoui, Z. and Chebbi, A.: Comparison of two kriging interpolation methods applied to spatiotemporal
876 rainfall, *J. Hydrol.*, 365(1–2), doi:10.1016/j.jhydrol.2008.11.025, 2009.

877 Koenker, R.: *Quantile Regression*, , doi:10.1017/CBO9780511754098, 2005.

878 Koutsoyiannis, D.: Statistics of extremes and estimation of extreme rainfall: I. Theoretical investigation, *Hydrol. Sci. J.*,
879 49(4), 575–590, doi:10.1623/hysj.49.4.575.54430, 2004a.

880 Koutsoyiannis, D.: Statistics of extremes and estimation of extreme rainfall: II. Empirical investigation of long rainfall
881 records, *Hydrol. Sci. J.*, 49(4), 591–610, doi:10.1623/hysj.49.4.591.54424, 2004b.

882 Koutsoyiannis, D., Kozonis, D. and Manetas, A.: A mathematical framework for studying rainfall intensity-duration-
883 frequency relationships, *J. Hydrol.*, 206(1–2), 118–135, doi:10.1016/S0022-1694(98)00097-3, 1998.

884 Lengfeld, K., Winterrath, T., Junghänel, T., Hafer, M. and Becker, A.: Characteristic spatial extent of hourly and daily
885 precipitation events in Germany derived from 16 years of radar data, *Meteorol. Zeitschrift*, 28(5), 363–378,
886 doi:10.1127/metz/2019/0964, 2019.

887 Licznar, P., De Michele, C. and Adamowski, W.: Precipitation variability within an urban monitoring network via
888 microcanonical cascade generators, *Hydrol. Earth Syst. Sci.*, 19(1), 485–506, doi:10.5194/hess-19-485-2015, 2015.

889 Lisniak, D., Franke, J. and Bernhofer, C.: Circulation pattern based parameterization of a multiplicative random cascade
890 for disaggregation of observed and projected daily rainfall time series, *Hydrol. Earth Syst. Sci.*, 17(7), 2487–2500,
891 doi:10.5194/hess-17-2487-2013, 2013.

892 Madsen, H., Arnbjerg-Nielsen, K. and Mikkelsen, P. S.: Update of regional intensity-duration-frequency curves in
893 Denmark: Tendency towards increased storm intensities, *Atmos. Res.*, 92(3), doi:10.1016/j.atmosres.2009.01.013,
894 2009.

895 Madsen, H., Gregersen, I. B., Rosbjerg, D. and Arnbjerg-Nielsen, K.: Regional frequency analysis of short duration
896 rainfall extremes using gridded daily rainfall data as co-variate, *Water Sci. Technol.*, 75(8), doi:10.2166/wst.2017.089,
897 2017.

898 Marra, F., Nikolopoulos, E. I., Anagnostou, E. N., Bárdossy, A. and Morin, E.: Precipitation frequency analysis from
899 remotely sensed datasets: A focused review, *J. Hydrol.*, 574(March), 699–705, doi:10.1016/j.jhydrol.2019.04.081,
900 2019.

901 Müller, H. and Haberlandt, U.: Temporal rainfall disaggregation using a multiplicative cascade model for spatial
902 application in urban hydrology, *J. Hydrol.*, 556, 847–864, doi:10.1016/J.JHYDROL.2016.01.031, 2018.

903 Olsson, J.: Evaluation of a scaling cascade model for temporal rain- fall disaggregation, *Hydrol. Earth Syst. Sci.*, 2(1),
904 19–30, doi:10.5194/hess-2-19-1998, 1998.

905 Paixao, ; E, Auld, H., Mirza, M. M. Q., Klaassen, J. and Shephard, M. W.: Regionalization of heavy rainfall to improve
906 climatic design values for infrastructure: case study in Southern Ontario, Canada, *Hydrol. Sci. Journal-Journal des Sci.*

Formatted: Italian (Italy)

907 Hydrol., 56(7), 1067–1089, doi:10.1080/02626667.2011.608069, 2011.

908 Papalexiou, S. M.: Unified theory for stochastic modelling of hydroclimatic processes: Preserving marginal
909 distributions, correlation structures, and intermittency, *Adv. Water Resour.*, 115, doi:10.1016/j.advwatres.2018.02.013,
910 2018.

911 Papalexiou, S. M. and Koutsoyiannis, D.: Battle of extreme value distributions : A global survey on extreme daily
912 rainfall, *Water Resour. Res.*, 49(1), 187–201, doi:10.1029/2012WR012557, 2013.

913 Pebesma, E. J.: Multivariable geostatistics in S: The *gstat* package, *Comput. Geosci.*, 30(7), 683–691,
914 doi:10.1016/j.cageo.2004.03.012, 2004.

915 Requena, A. I., Burn, D. H. and Coulibaly, P.: Pooled frequency analysis for intensity–duration–frequency curve
916 estimation, *Hydrol. Process.*, 33(15), doi:10.1002/hyp.13456, 2019.

917 De Salas, L. and Fernández, J. A.: “In-site” regionalization to estimate an intensity-duration-frequency law: a solution
918 to scarce spatial data in Spain, *Hydrol. Process. Hydrol. Process*, 21, 3507–3513, doi:10.1002/hyp.6551, 2007.

919 Shehu, B. and Haberlandt, U.: Uncertainty estimation of regionalised depth-duration-frequency curves in Germany,
920 *Hydrol. Earth Syst. Sci.*, [preprint], in review, doi:https://doi.org/10.5194/hess-2022-254, 2022.

921 Smithers, J. C. and Schulze, R. E.: A methodology for the estimation of short duration design storms in South Africa
922 using a regional approach based on L-moments, *J. Hydrol.*, 241(1–2), doi:10.1016/S0022-1694(00)00374-7, 2001.

923 Uboldi, F., Sulis, A. N., Lussana, C., Cislighi, M. and Russo, M.: A spatial bootstrap technique for parameter
924 estimation of rainfall annual maxima distribution, *Hydrol. Earth Syst. Sci.*, 18(3), 981–995, doi:10.5194/hess-18-981-
925 2014, 2014.

926 Ulrich, J., Jurado, O. E., Peter, M., Scheibel, M. and Rust, H. W.: Estimating idf curves consistently over durations with
927 spatial covariates, *Water (Switzerland)*, 12(11), 1–22, doi:10.3390/w12113119, 2020.

928 Ulrich, J., Fauer, F. S. and Rust, H. W.: Modeling seasonal variations of extreme rainfall on different timescales in
929 Germany, *Hydrol. Earth Syst. Sci.*, 25(12), doi:10.5194/hess-25-6133-2021, 2021.

930 Viglione, A., Hosking, J. R. M., Laio, F., Miller, A., Gaume, E., Payrastra, O., Salinas, J. L., N’guyen, C. C. and
931 Halbert, K.: Non-Supervised Regional Flood Frequency Analysis., 2020.

932 Van de Vyver, H.: Bayesian estimation of rainfall intensity-duration-frequency relationships, *J. Hydrol.*, 529,
933 doi:10.1016/j.jhydrol.2015.08.036, 2015.

934 Van De Vyver, H.: Spatial regression models for extreme precipitation in Belgium, *Water Resour. Res.*, 48(9), 1–17,
935 doi:10.1029/2011WR011707, 2012.

936 Ward, J. H.: Hierarchical Grouping to Optimize an Objective Function, *J. Am. Stat. Assoc.*, 58(301), 236–244,
937 doi:10.1080/01621459.1963.10500845, 1963.

938 Watkins, D. W., Link, G. A. and Johnson, D.: Mapping regional precipitation intensity duration frequency estimates, *J.*
939 *Am. Water Resour. Assoc.*, 41(1), doi:10.1111/j.1752-1688.2005.tb03725.x, 2005.

940



Figure A1 Cross-correlation between the selected local parameters (Koutsoyiannis and GEV parameters) for regionalisation and useful site characteristics that might act as an external drift information. Mu is the location parameter, sigma the scale parameter, theta and eta the Koutsoyiannis parameters, ELEV is short for elevation information, SUN is short for long term average of annual sunshine duration, PCP is short for long term average of annual rainfall amount, and TEMP is short for the long-term average of annual mean temperature.

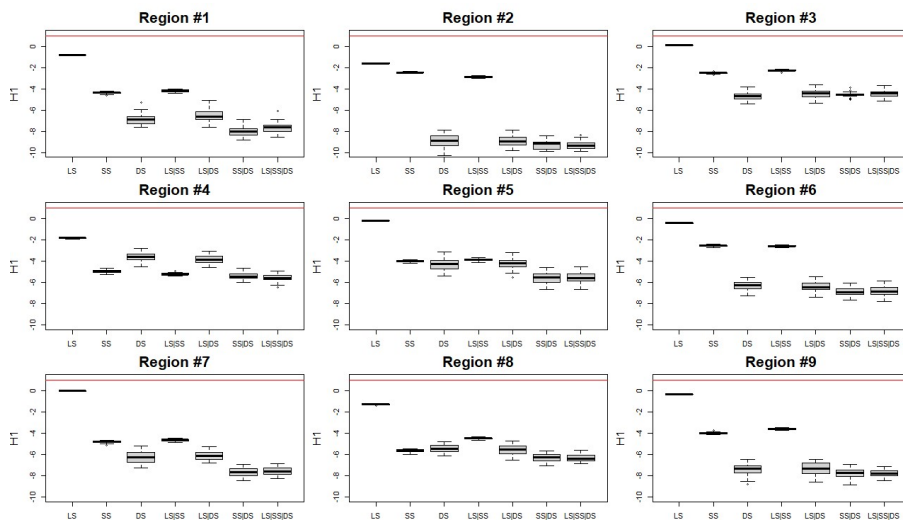


Figure A2 The homogeneity index (HI) computed for each of the 9th selected regions for each of the dataset combinations.

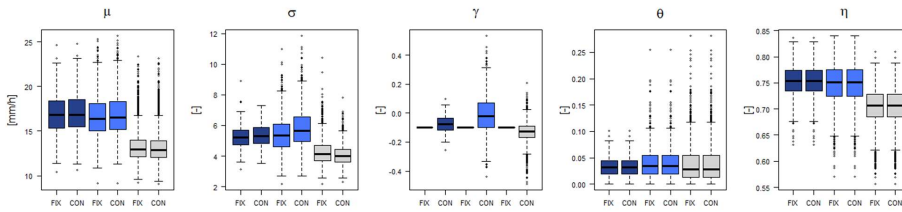


Figure A3 Koutsoyiannis parameters obtained for each data set (LS in dark blue, SS in light blue and DS in grey) when fixing the shape parameter to 0.1 (FIX) or letting it free (FREE).

945

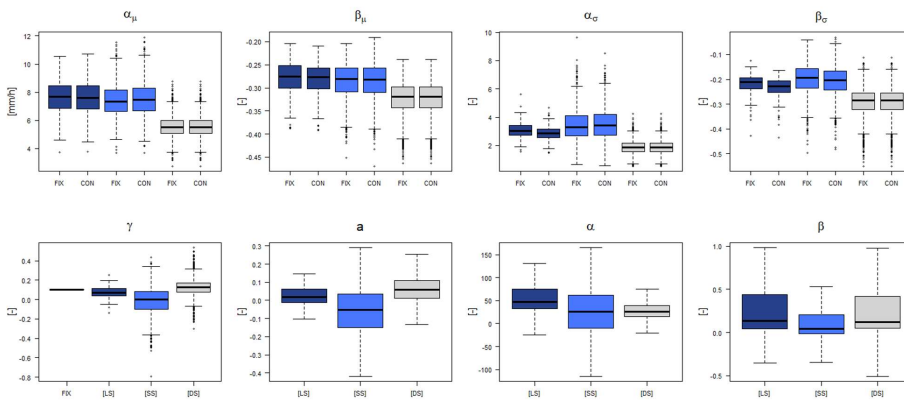


Figure A4 Fischer/Schumann parameters obtained for each data set (LS in dark blue, SS in light blue and DS in grey) when fixing the shape parameter to 0.1 (FIX) or letting it free (FREE).

946

	RMSE (%)					PBIAS (%)					NSE (%)				
	T1a	T10a	T20a	T50a	T100a	T1a	T10a	T20a	T50a	T100a	T1a	T10a	T20a	T50a	T100a
SS	8.5	0.4	0.5	-8.1	-12.0	0.3	8.1	5.1	-1.2	-6.1	0.1	0.4	-0.3	-0.3	-0.6
DS	-53.1	-42.2	-40.9	-36.4	-34.3	-59.3	-35.7	-26.6	-25.8	-21.2	-2.6	-1.8	-1.8	-1.8	-1.8
SS + DS	9.6	-1.0	-0.6	-3.3	-5.0	2.2	-3.9	-1.6	-5.6	-8.8	0.5	0.2	-0.1	-0.1	-0.3

Figure A54 Fischer/Schumann parameters obtained for each data set (LS in dark blue, SS in light blue and DS in grey) when fixing the shape parameter to 0.1 (FIX) or letting it free (FREE). Obtained Deterioration (-) or Improvement (+) towards the best regionalisation technique (KED[LS|SS]) when no long data series are available (LS) and the regionalisation is performed based on short series (SS), disaggregated daily series (DS), or on both SS and DS.

947

948

Formatted: Font: Bold, Check spelling and grammar